
Semiconductor Devices

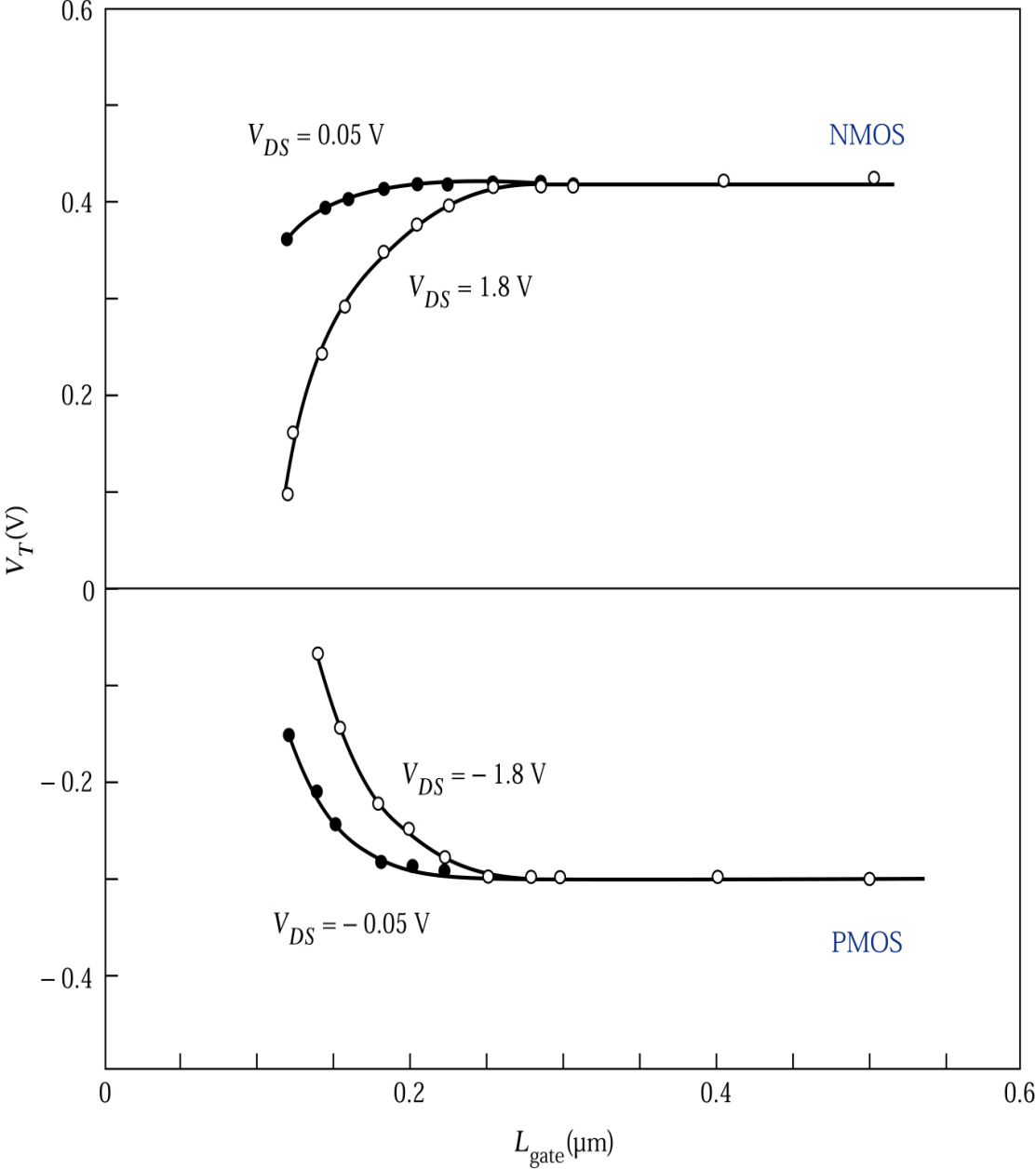
THIRD EDITION

S. M. Sze and M. K. Lee

Chapter 6

Advanced MOSFET and Related Devices

Figure 6.1. Threshold voltage **roll-off** characteristics in a 0.15 μm complementary metal-oxide-semiconductor (CMOS) field-effect transistor technology.⁷



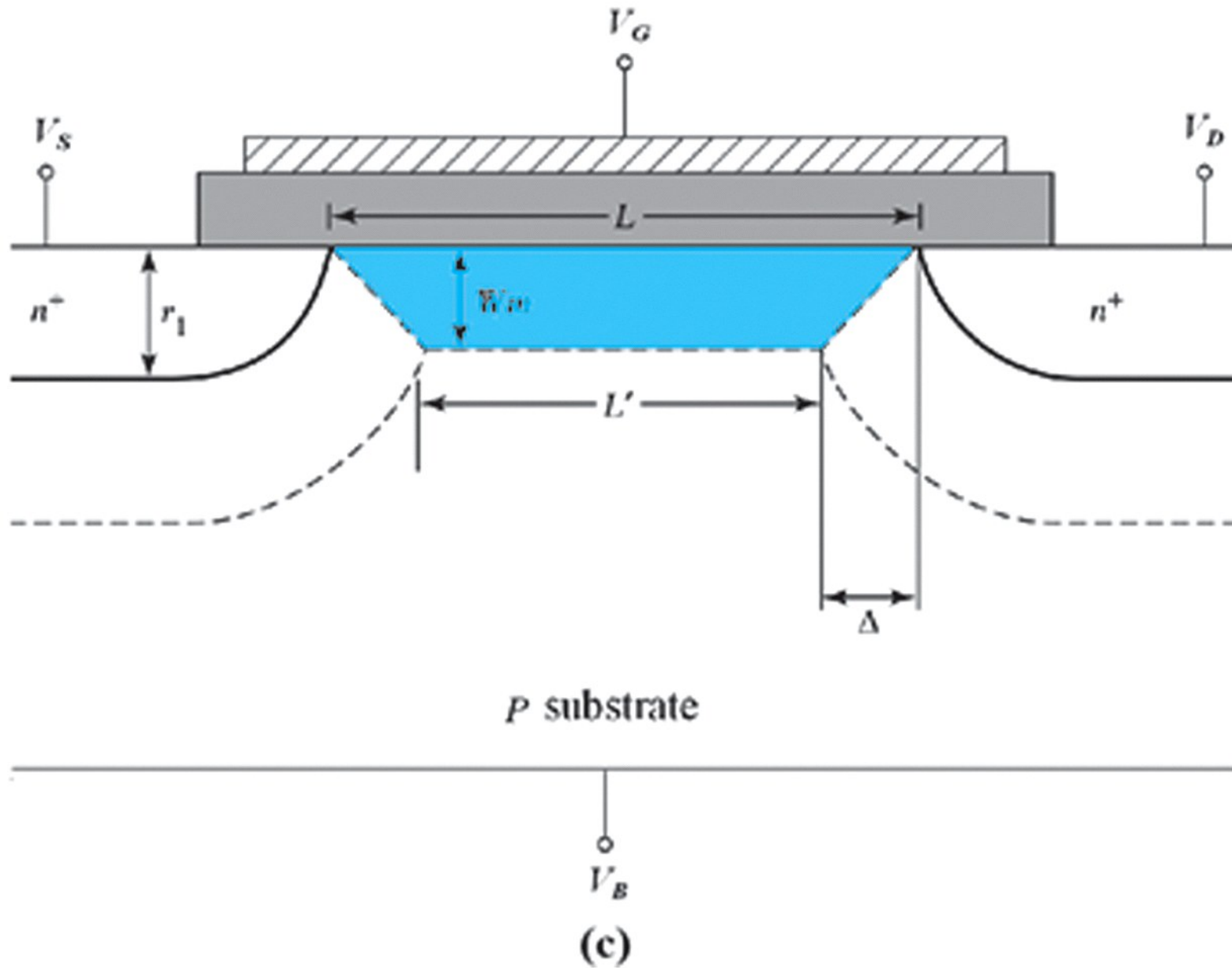
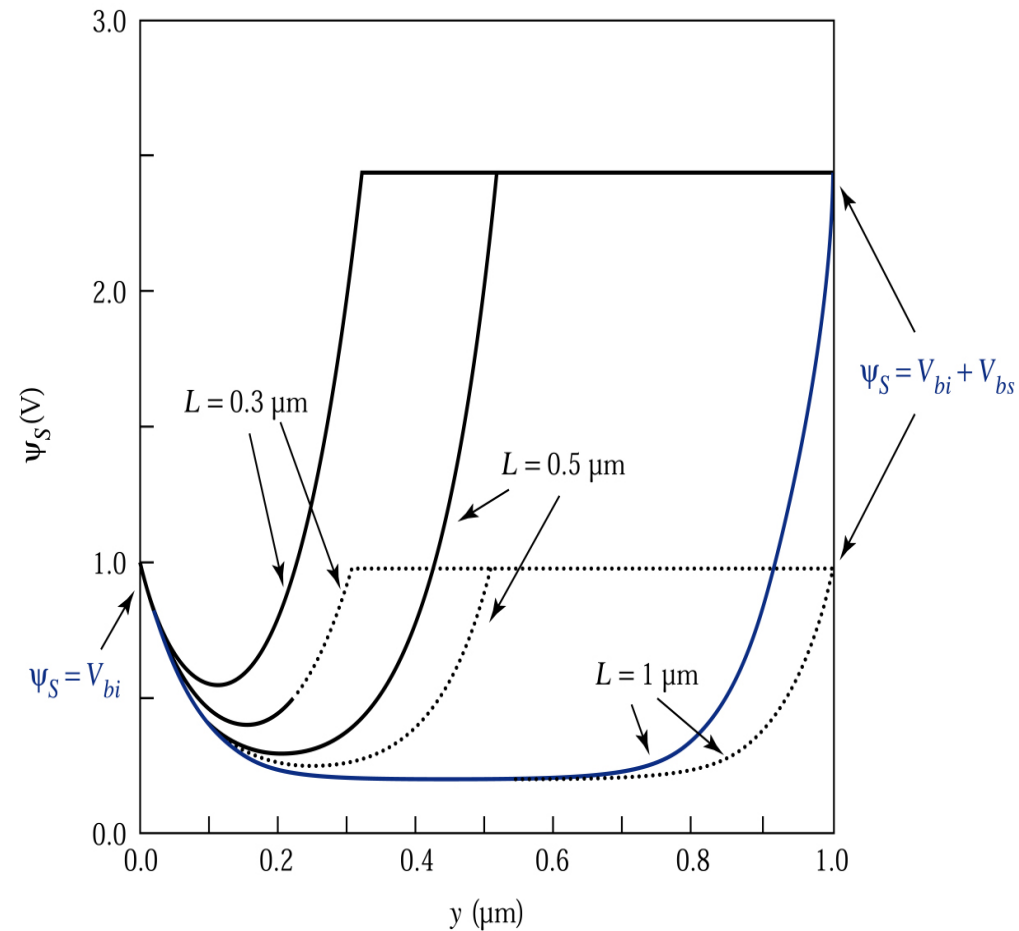
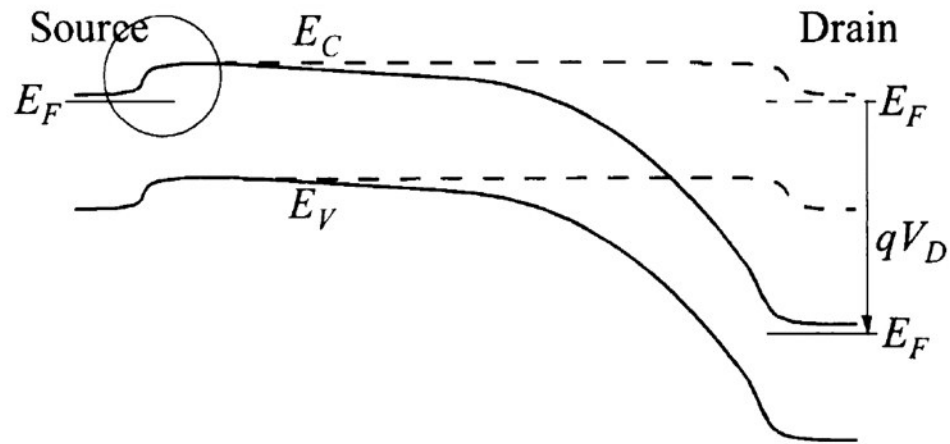


Figure 6.2c
 © John Wiley & Sons, Inc. All rights reserved.

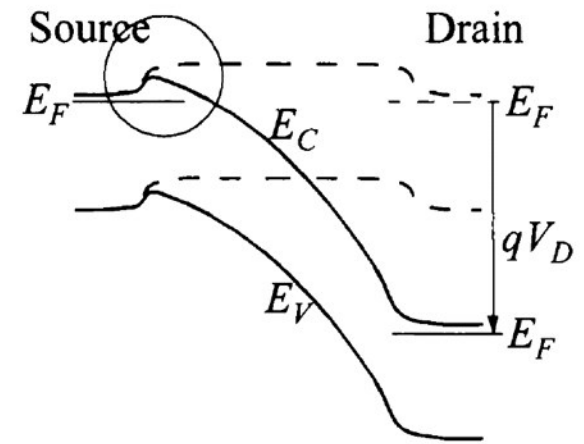
Schematic of the **charge sharing** model.⁸



Calculated surface potential along the channel for n -channel MOSFETs with different channel lengths.⁹ The source-channel boundary is at $y = 0$. A **low (0.05 V, dotted lines) and a high (1.5 V, solid lines) V_{DS}** are applied. Oxide thickness d and substrate doping N_A are 10 nm and 10^{16} cm^{-3} , respectively. The substrate bias is 0 V.



(a)



(b)

Figure 6.3
© John Wiley & Sons, Inc. All rights reserved.

Band diagram from source to drain, (a) long L , (b) short L ,
dash line: $V_D = 0$, solid line: $V_D > 0$

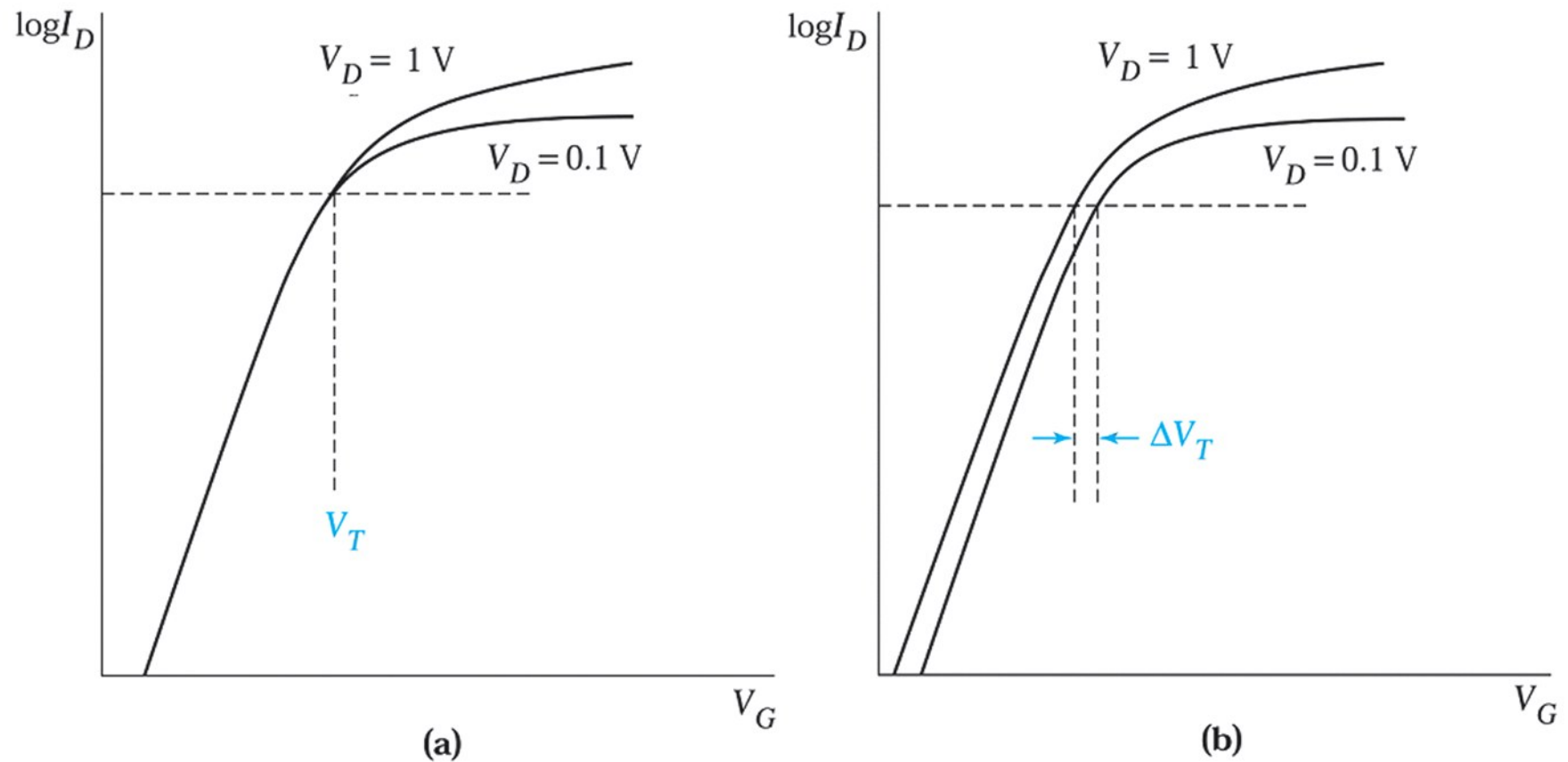
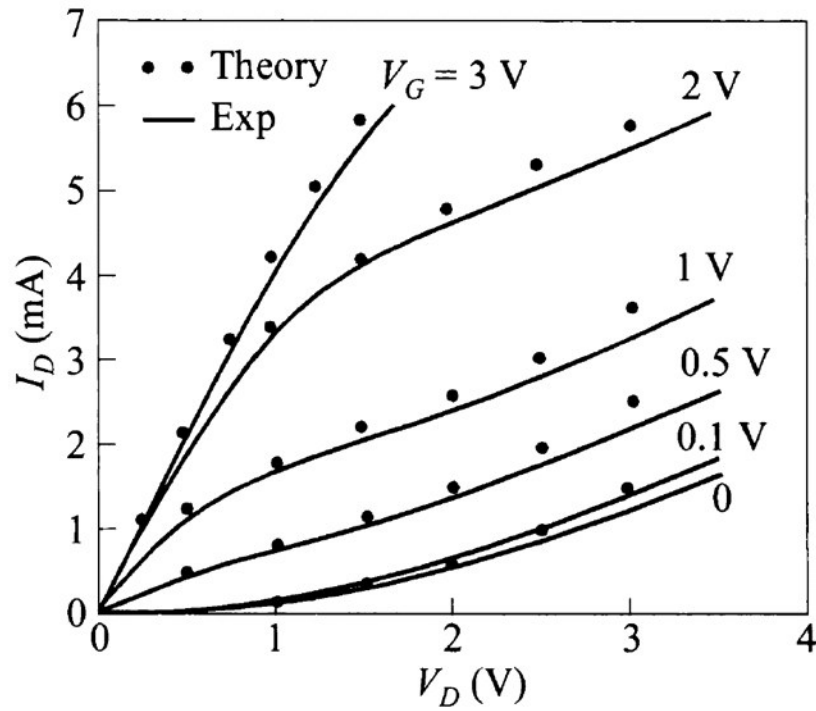


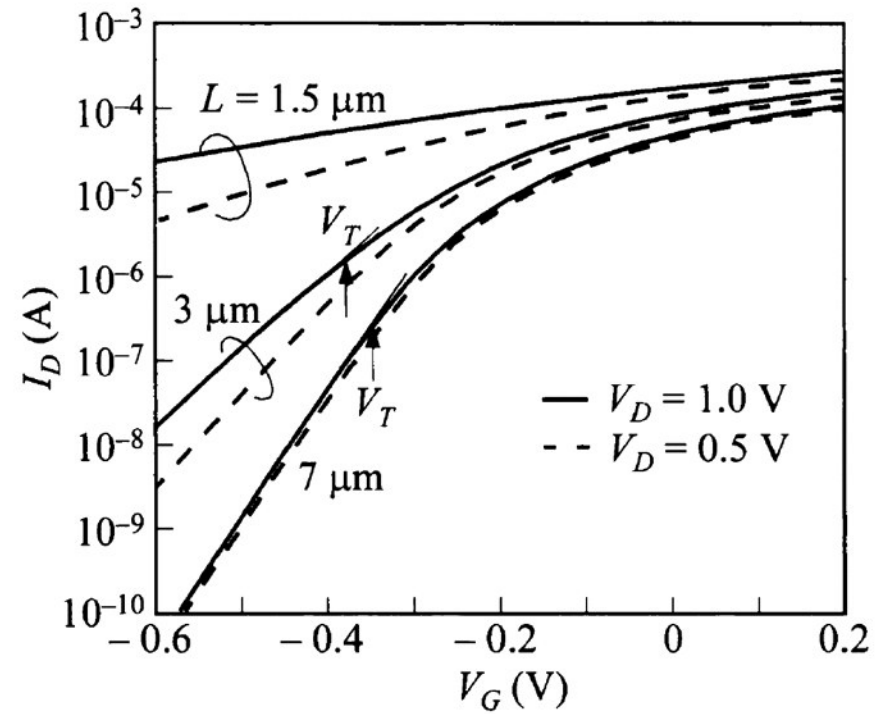
Figure 6.4
 © John Wiley & Sons, Inc. All rights reserved.

Figure 6.4.
 Subthreshold characteristics of
 (a) a long-channel and
 (b) a short-channel MOSFET.

DIBL: Drain-Induced Barrier Lowering



(a)



(b)

Figure 6.5
© John Wiley & Sons, Inc. All rights reserved.

Punch-through, (a) above threshold, (b) below threshold

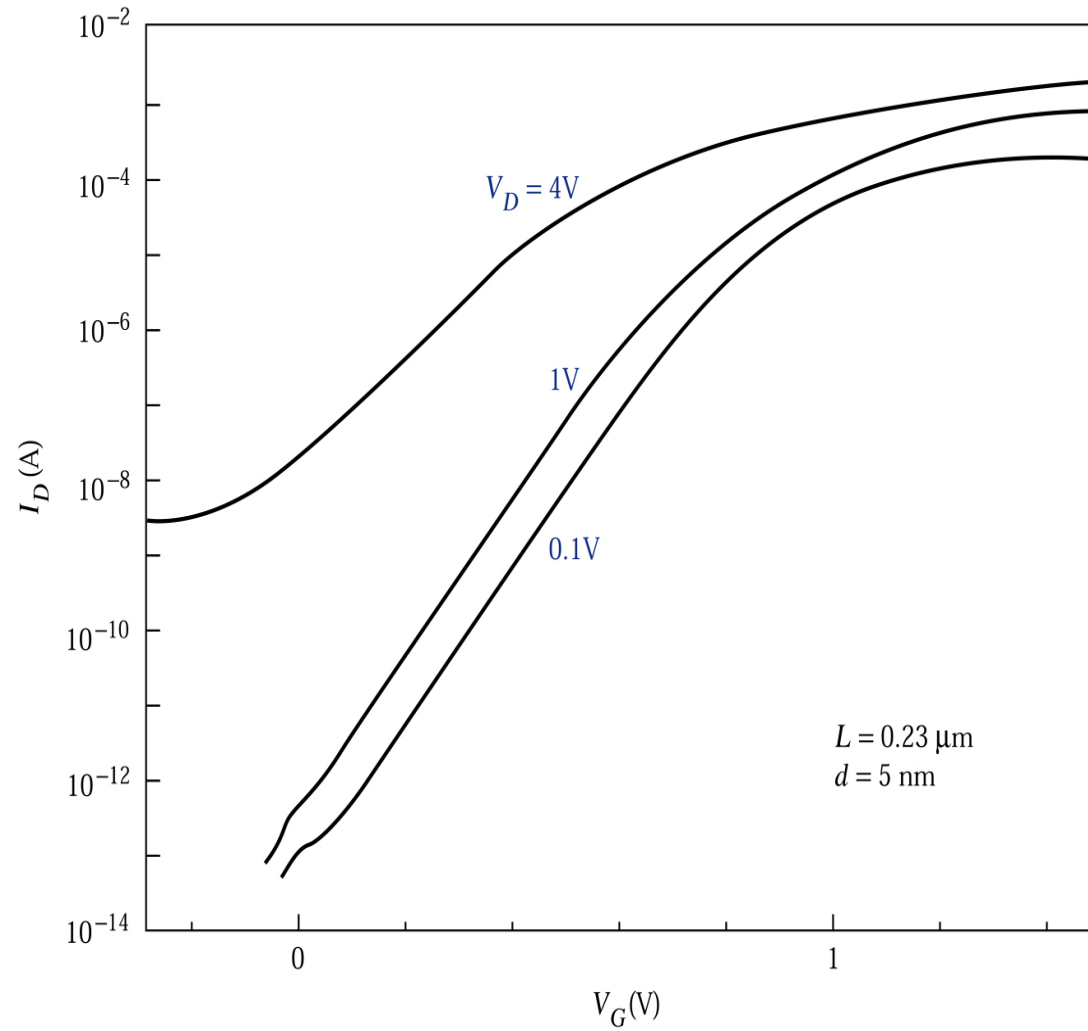


Figure 6.6. Subthreshold characteristics of an n -channel MOSFET with $V_{DS} = 0.1, 1, \text{ and } 4 \text{ V}$.

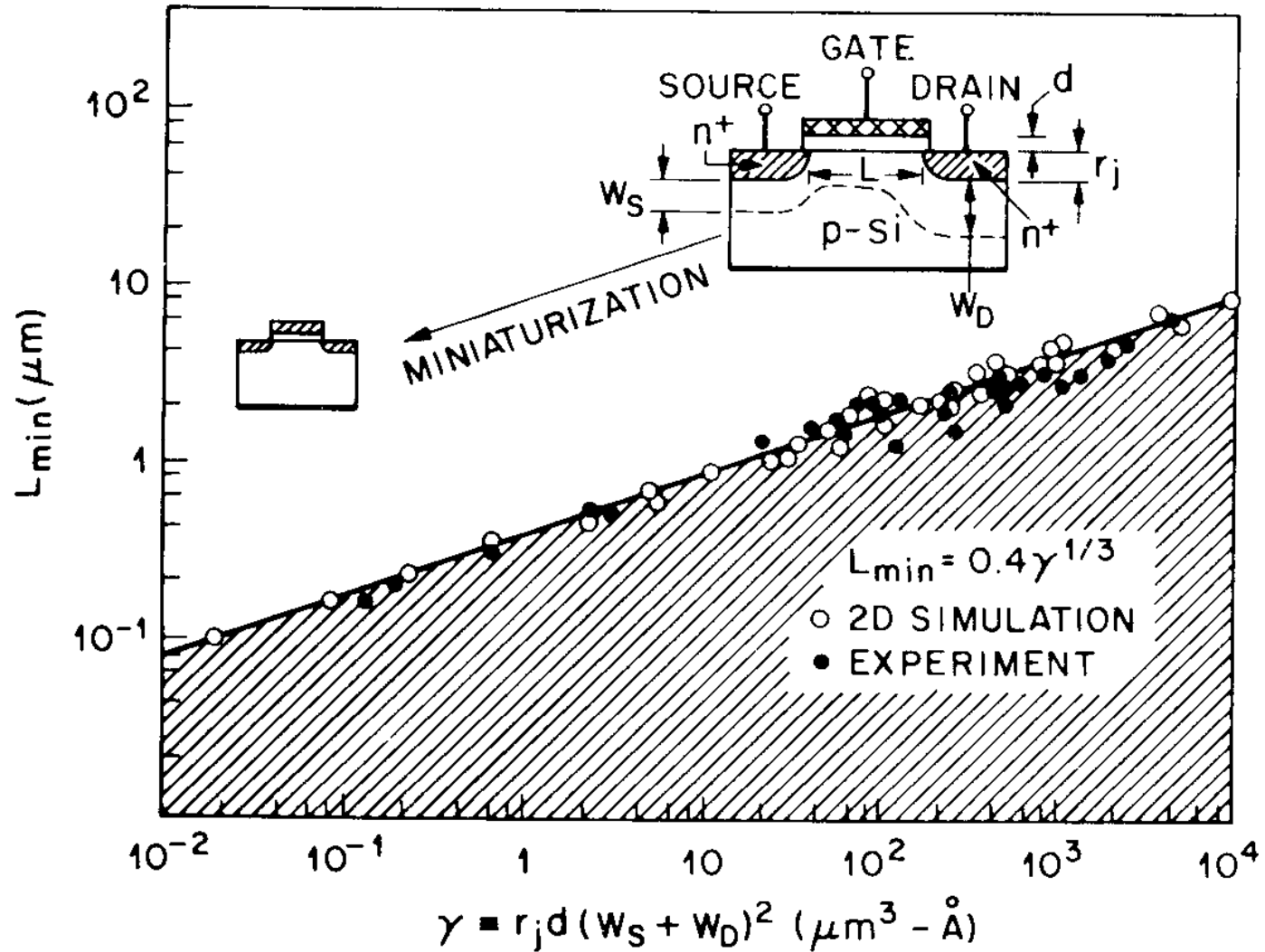
TABLE 1 Scaling of MOSFET Device and Circuit Parameters

Determinant	MOSFET device and circuit parameters	Multiplying factor ($\kappa > 1$)
Scaling assumptions	Device dimensions (d, L, W, r_j)	$1/\kappa$
	Doping concentration (N_A, N_D)	κ
	Voltage (V)	$1/\kappa$
Derived scaling behavior of device parameters	Electric field (\mathcal{E})	1
	Carrier velocity (v)	1
	Depletion-layer width (W)	$1/\kappa$
	Capacitance ($C = \epsilon A/d$)	$1/\kappa$
	Inversion-layer charge density (Q_n)	1
	Current, drift (I)	$1/\kappa$
	Channel resistance (R)	1
Derived scaling behavior of circuit parameters	Circuit delay time ($\tau \sim CV/I$)	$1/\kappa$
	Power dissipation per circuit ($P \sim VI$)	$1/\kappa^2$
	Power-delay product per circuit ($P\tau$)	$1/\kappa^3$
	Circuit density ($\sim 1/A$)	κ^2
	Power density (P/A)	1

Table 6.1

© John Wiley & Sons, Inc. All rights reserved.

Scaling of MOS counts on d , r_j , or W_d/W_s



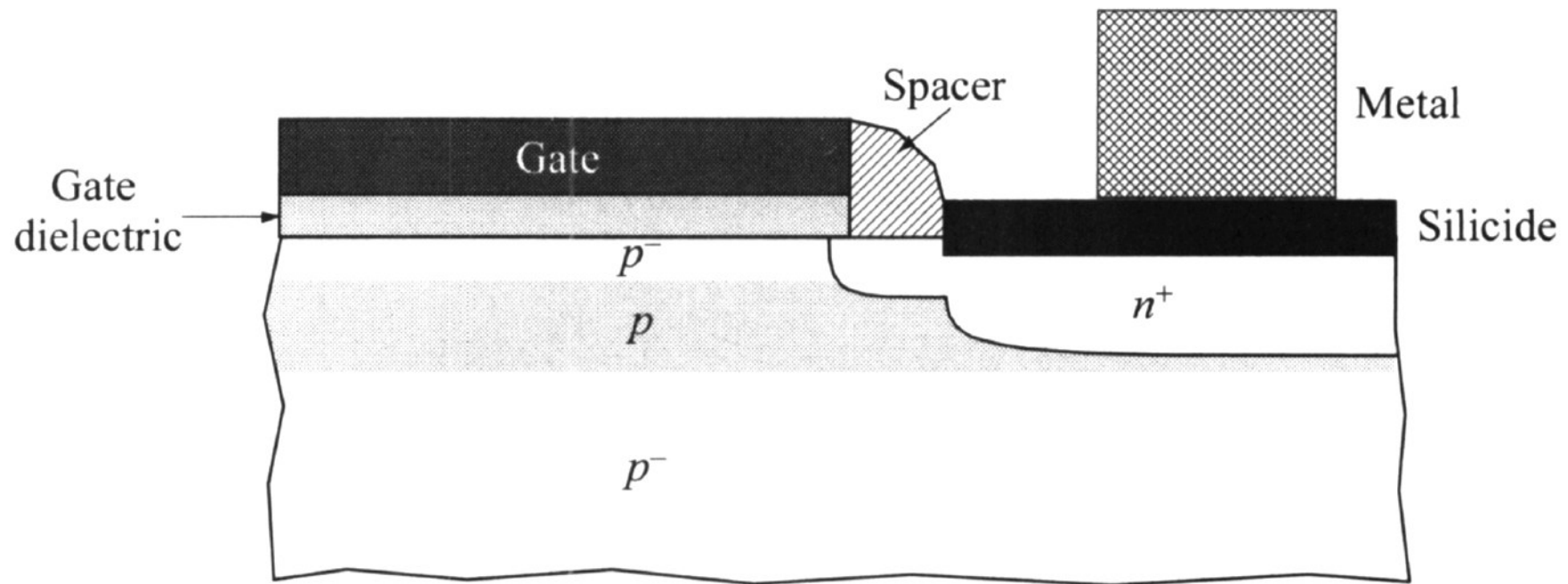


Figure 6.7
 © John Wiley & Sons, Inc. All rights reserved.

Retrograde channel doping profile

Upper P^- : mobility improvement

Middle P : control punch-through, short L effects

Bottom P^- : reduce C_j , body effect

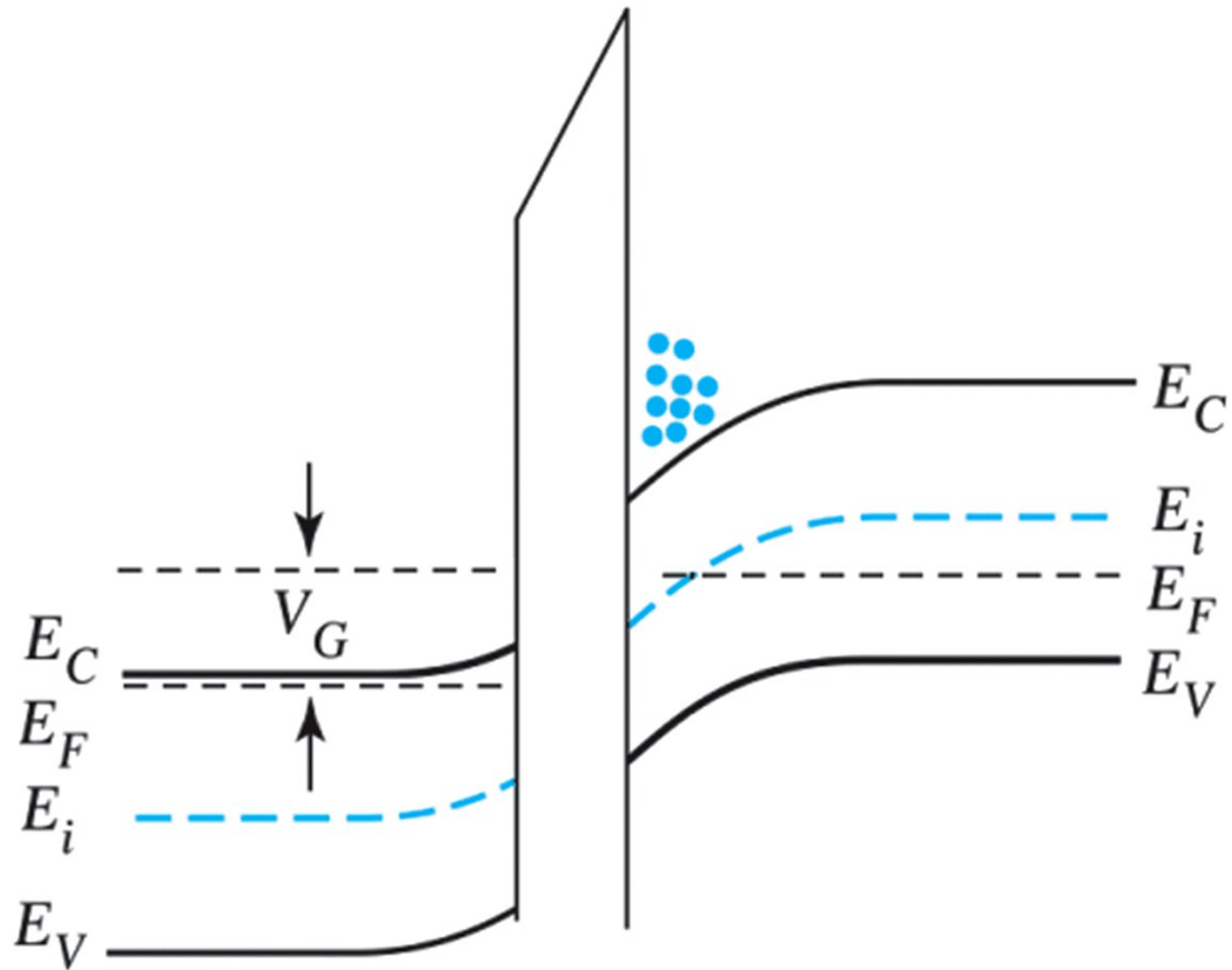


Figure 6.8a
 © John Wiley & Sons, Inc. All rights reserved.

poly-Si gate depletion effects

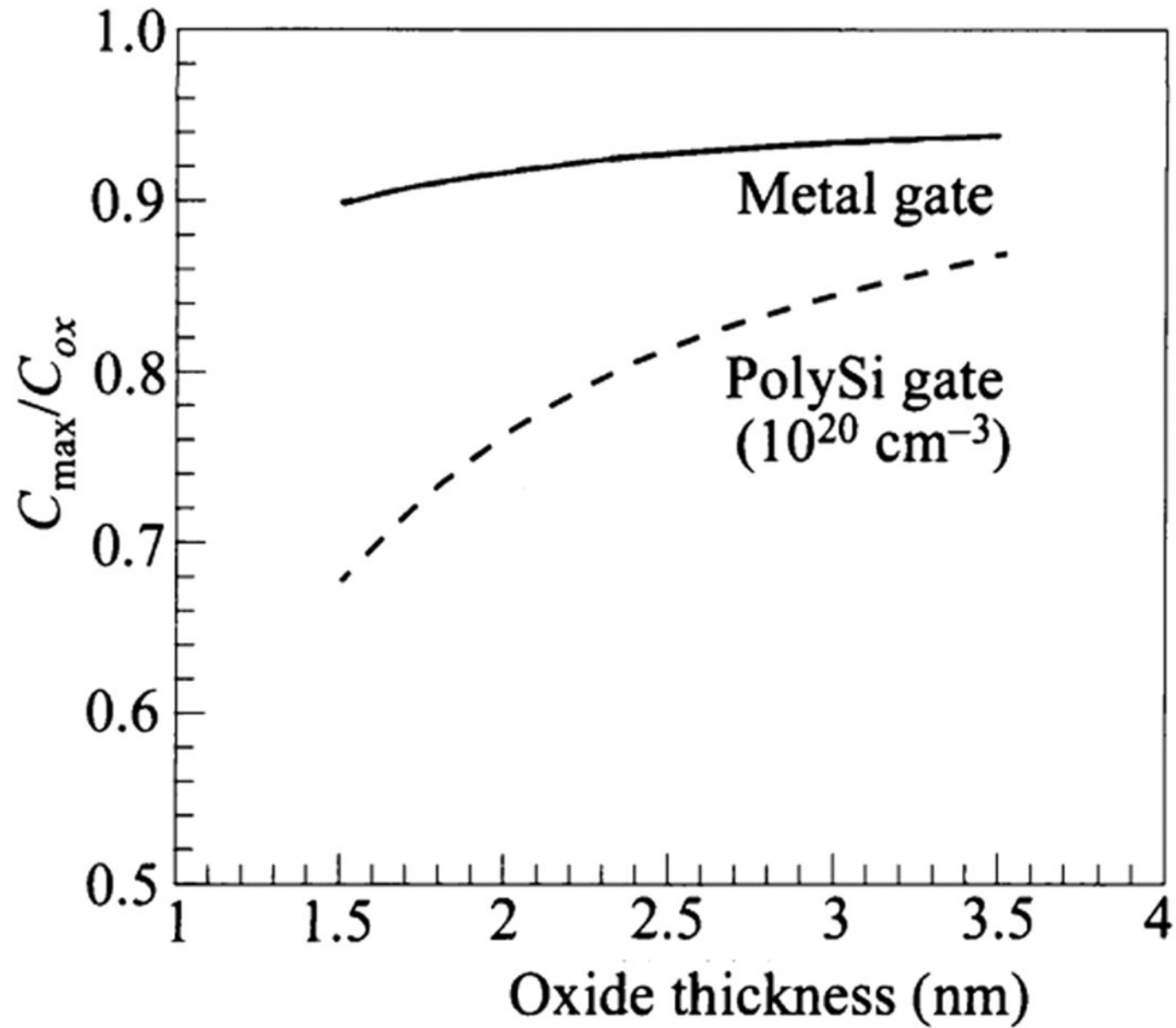


Figure 6.8b
© John Wiley & Sons, Inc. All rights reserved.

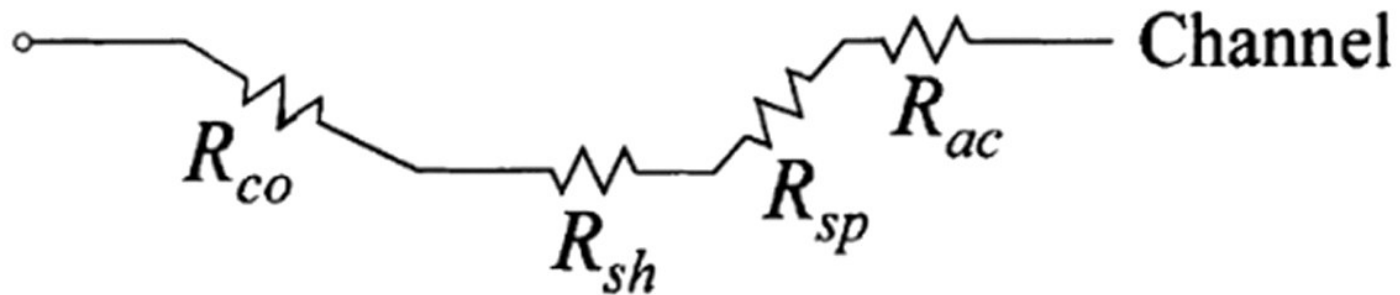
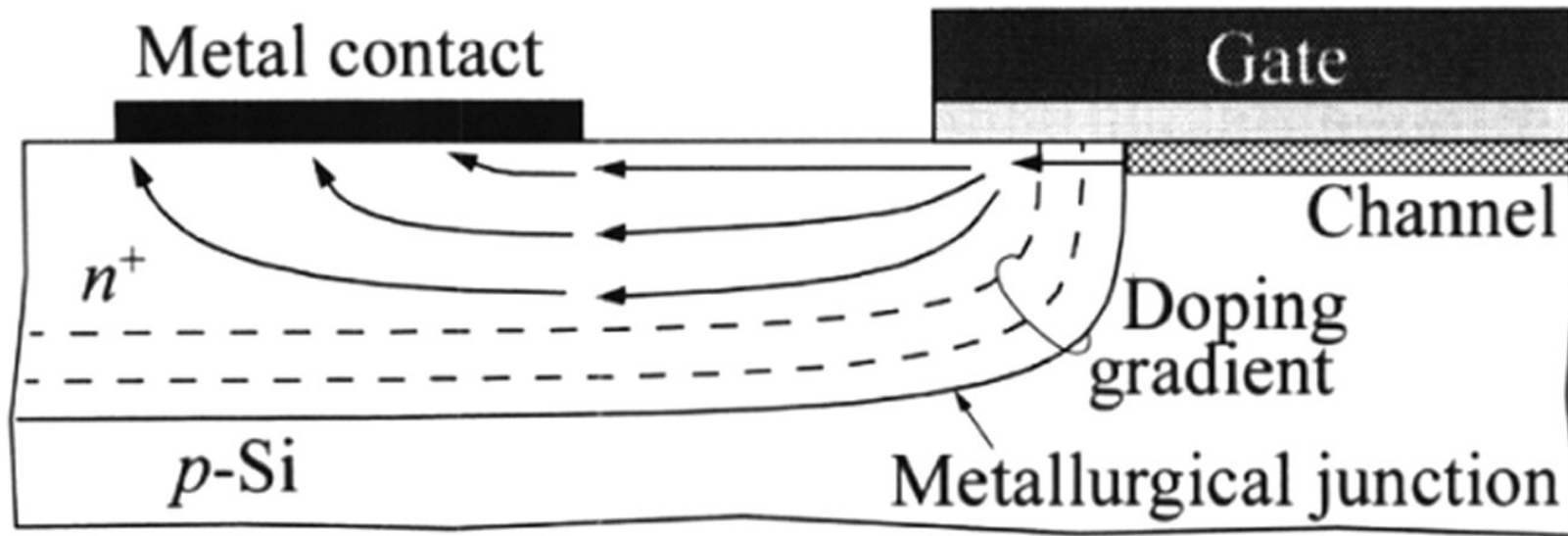


Figure 6.9
 © John Wiley & Sons, Inc. All rights reserved.

Different components of parasitic S/D series resistance

Schottky-barrier S/D

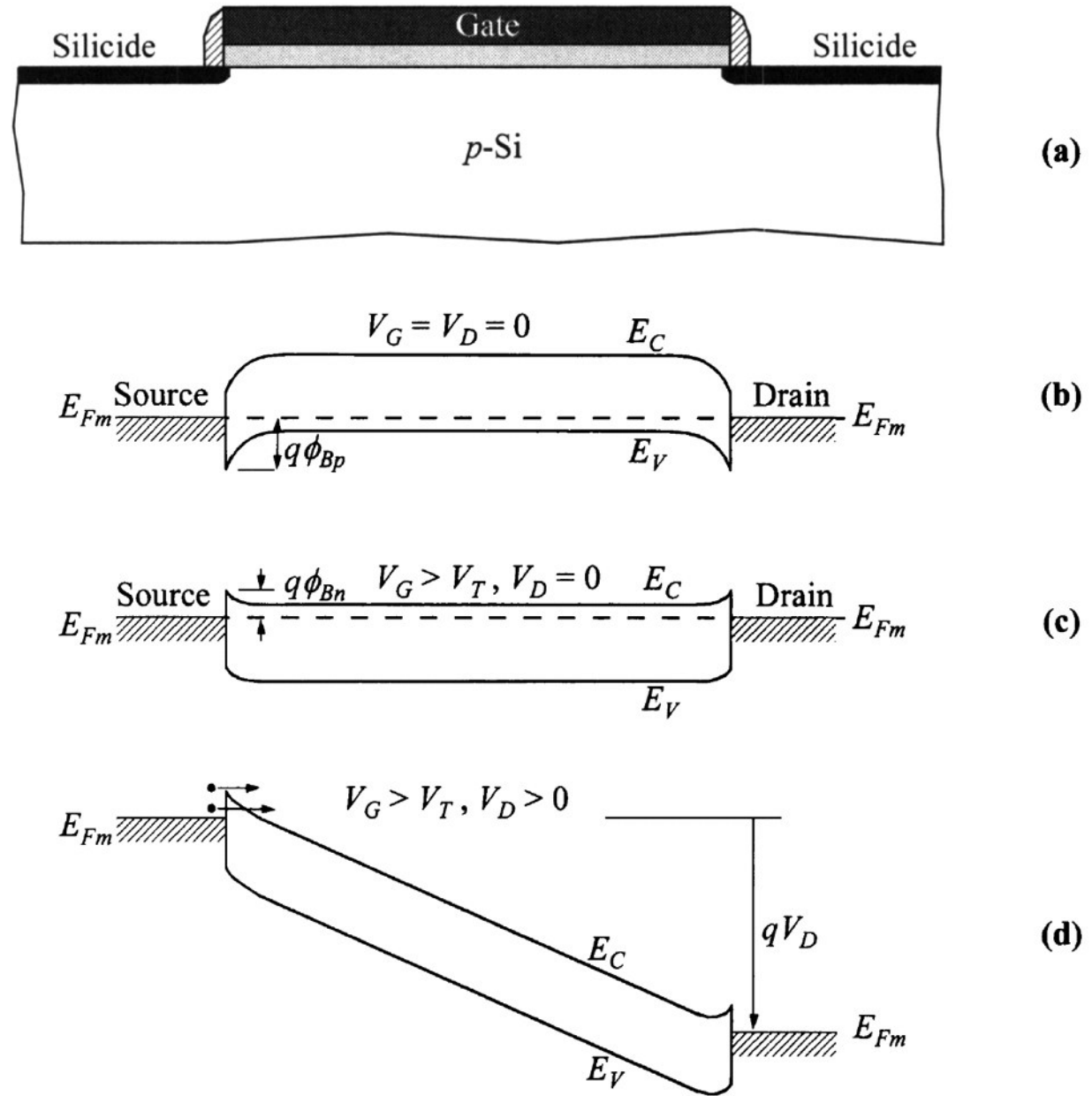


Figure 6.10
 © John Wiley & Sons, Inc. All rights reserved.

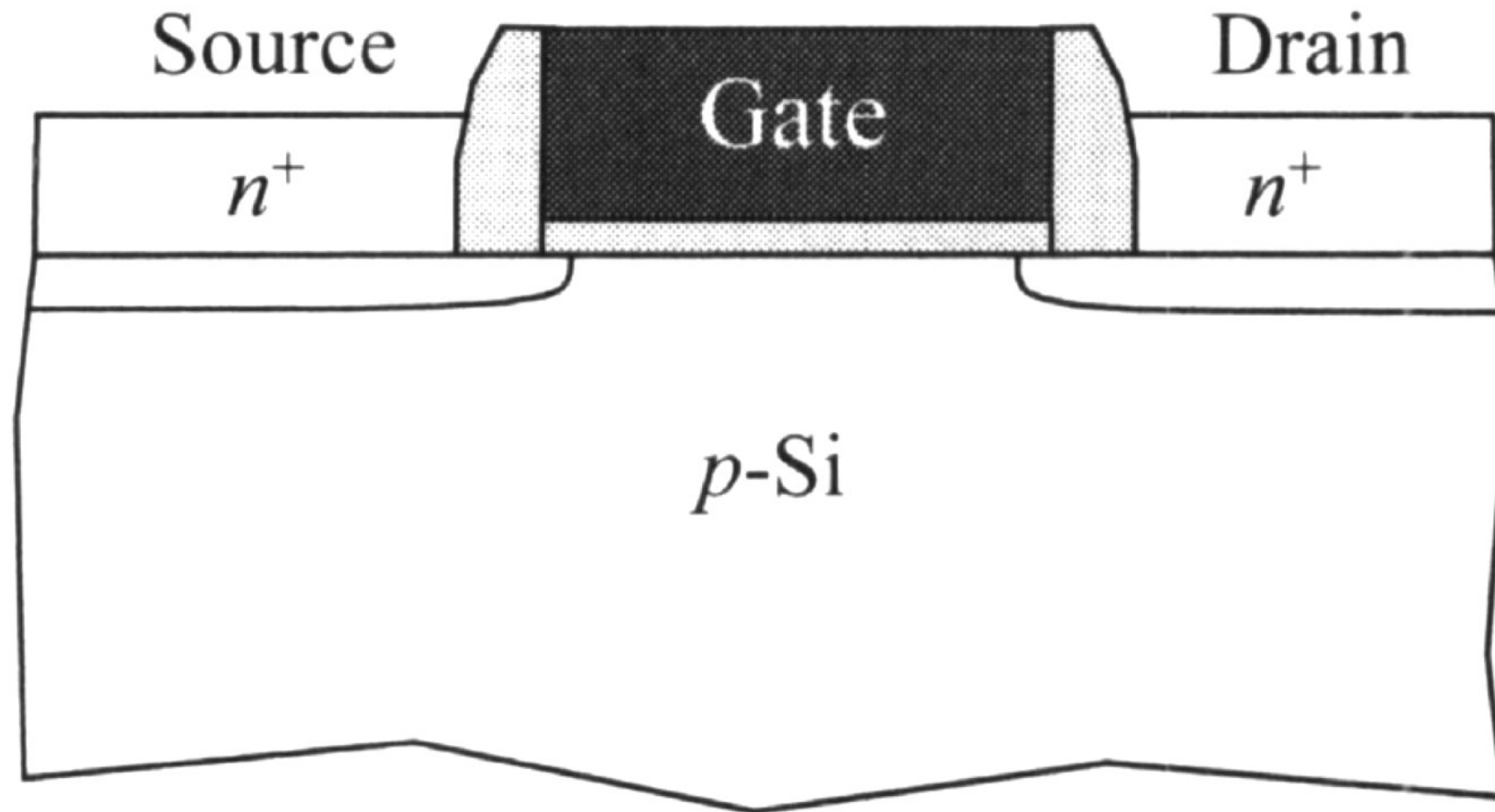
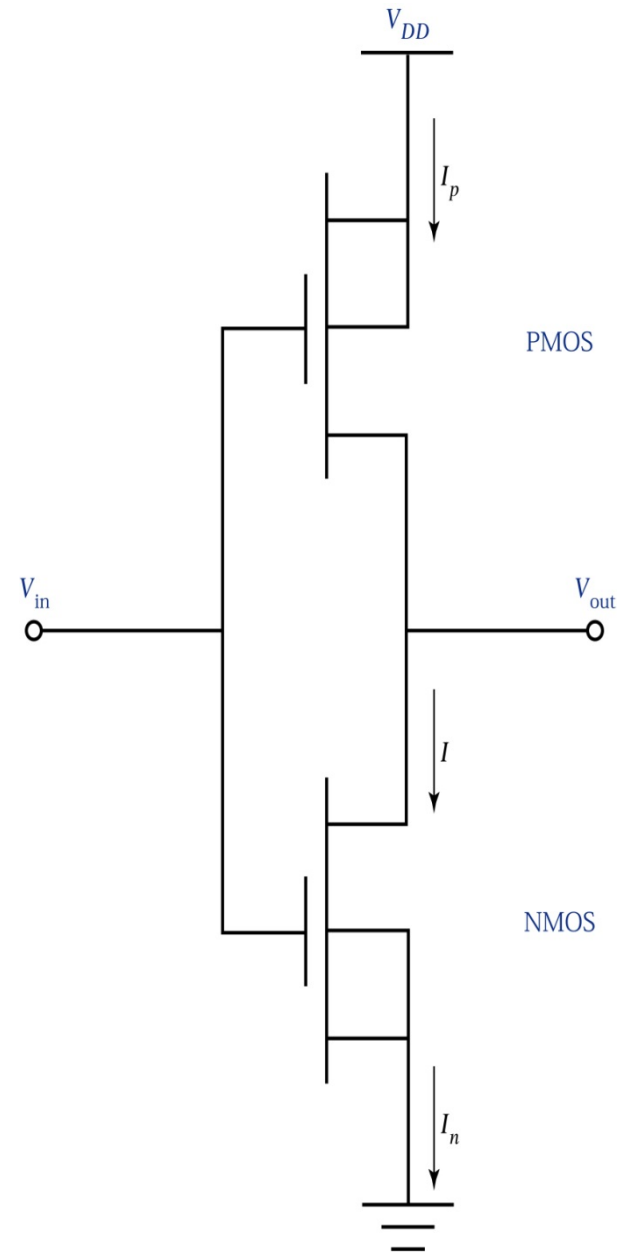


Figure 6.11
© John Wiley & Sons, Inc. All rights reserved.

Raised S/D to reduce junction depth and series resistance

Figure 6.12. The CMOS inverter.



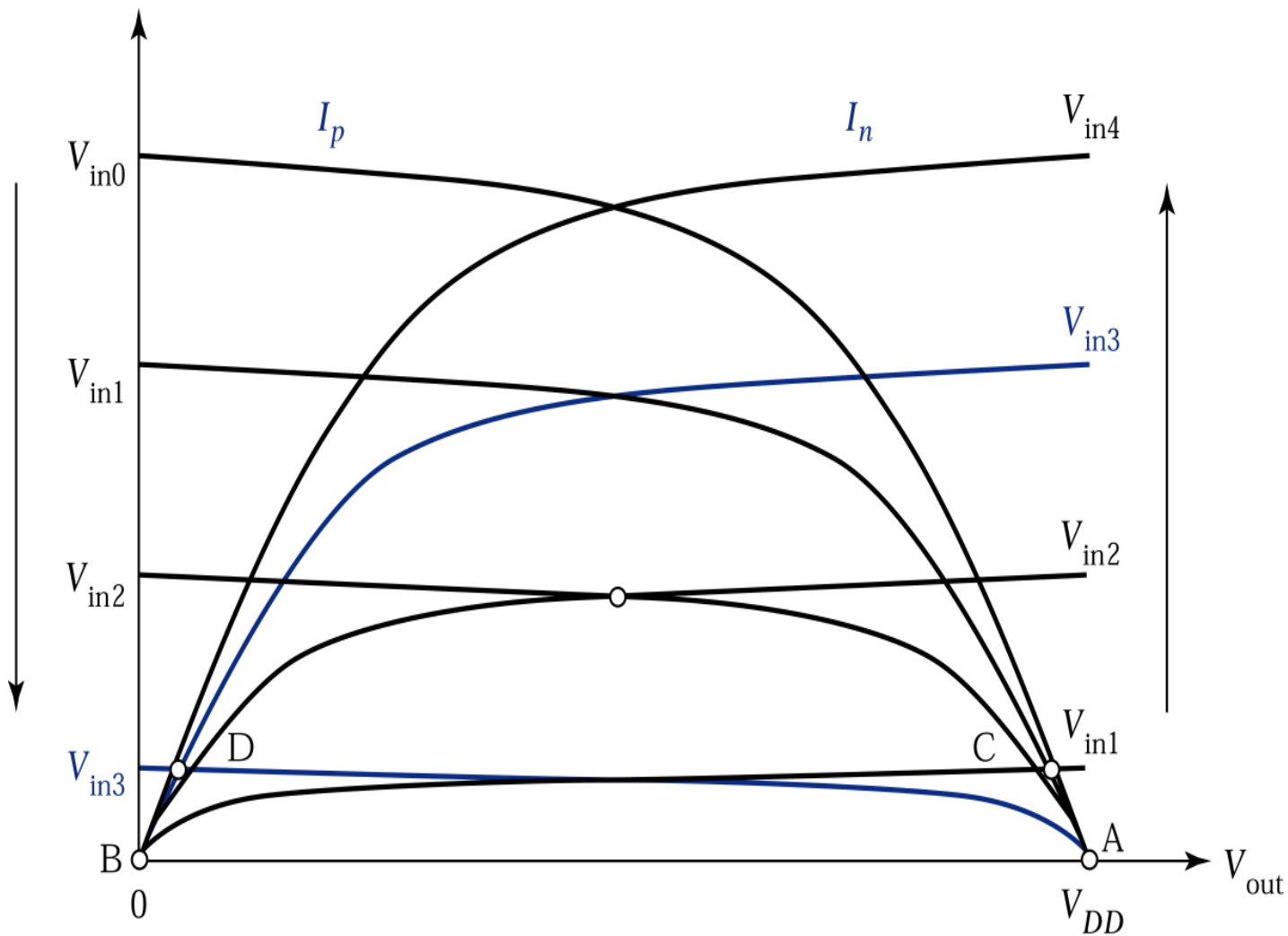
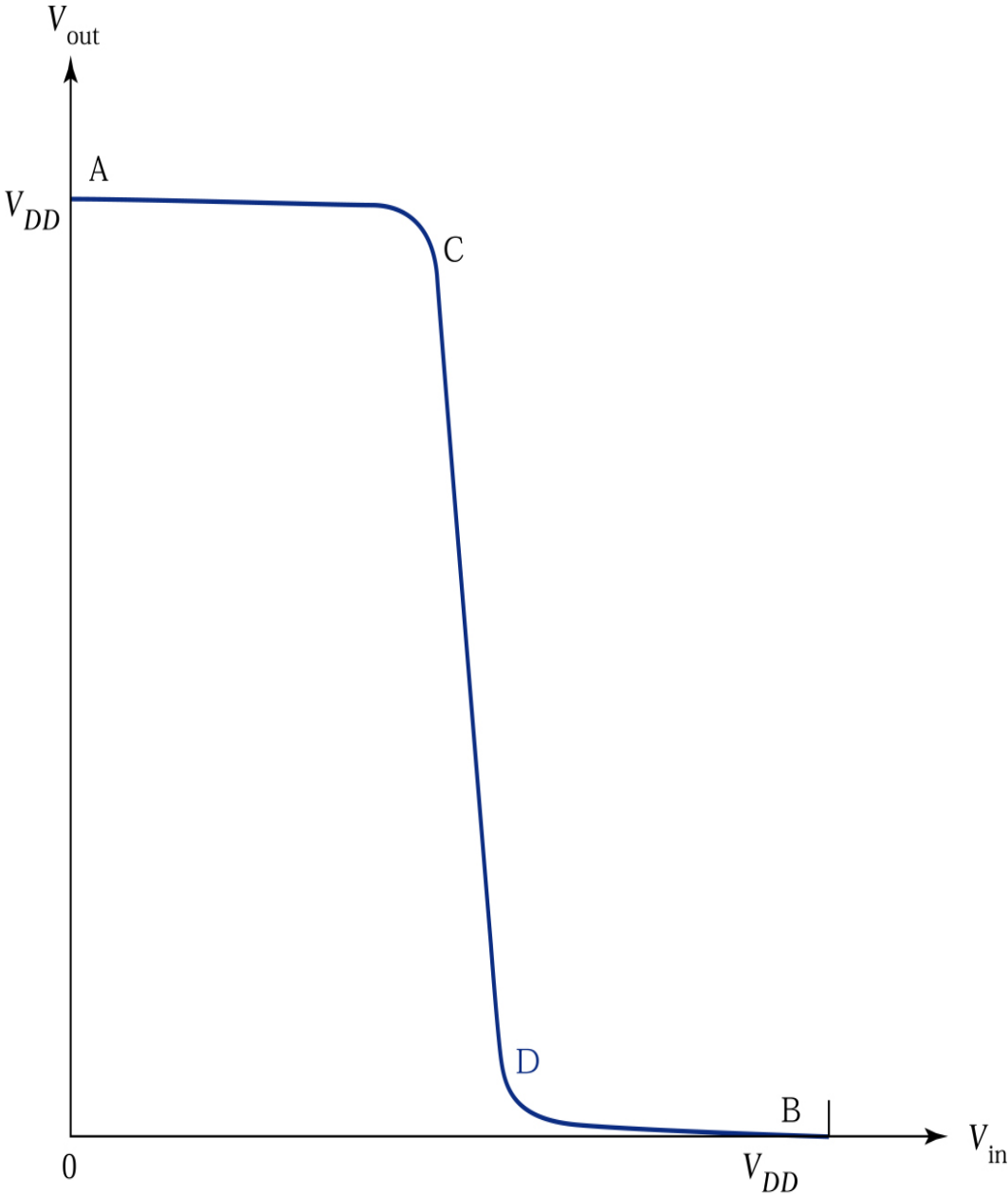


Figure 6.13. I_p and I_n as a function of V_{out} . The intercepts of I_p and I_n (circled) represent the steady-state operation points of the CMOS inverter.¹¹ The curves are labeled by the input voltages: $0 = V_{in0} < V_{in1} < V_{in2} < V_{in3} < V_{in4} = V_{DD}$.

Figure 6.14.

Transfer curve of a CMOS inverter.¹¹

Points labeled A, B, C, and D correspond to those points labeled in Fig. 13.



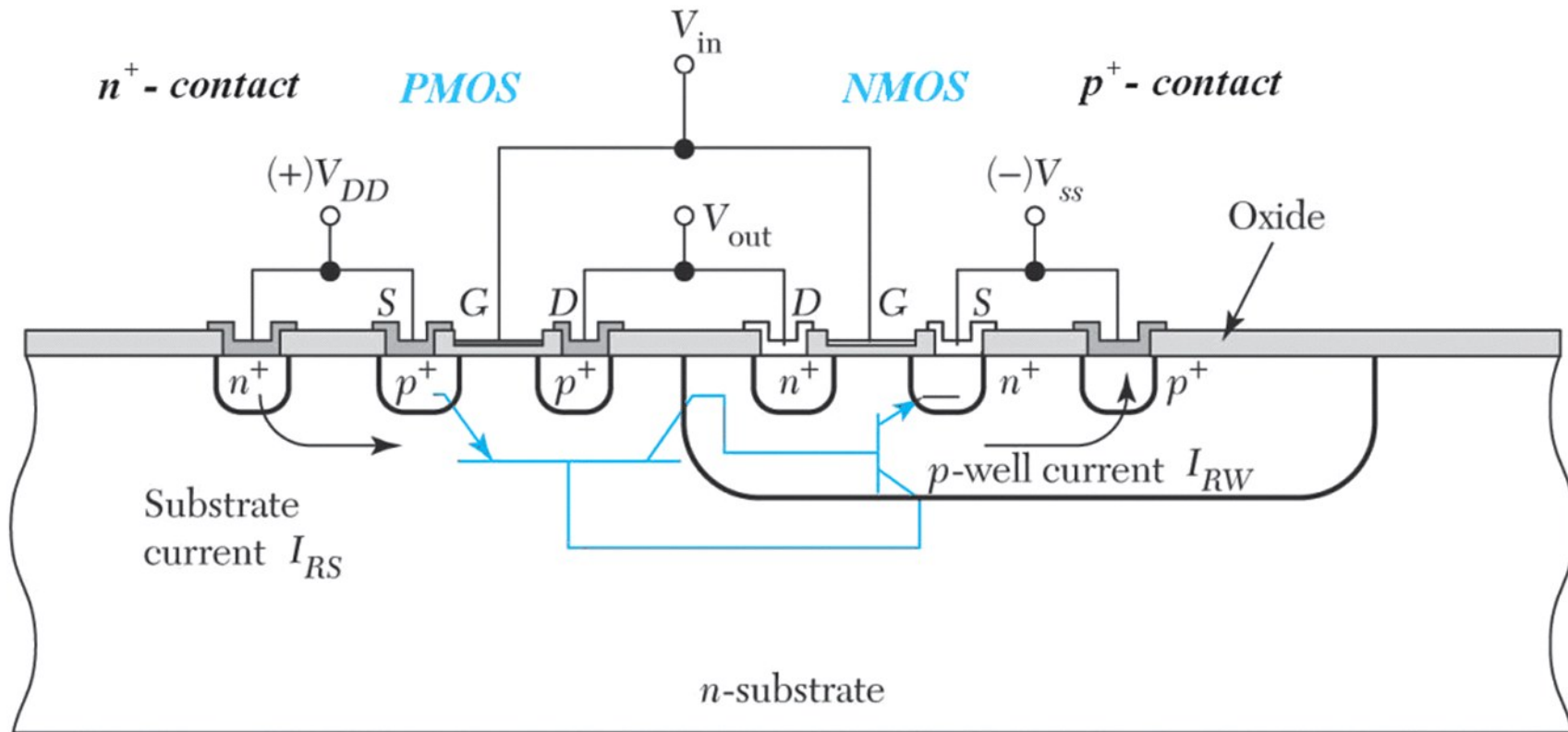


Figure 6.15
 © John Wiley & Sons, Inc. All rights reserved.

Figure 6.15. Cross section of a CMOS inverter fabricated with p -well technology.

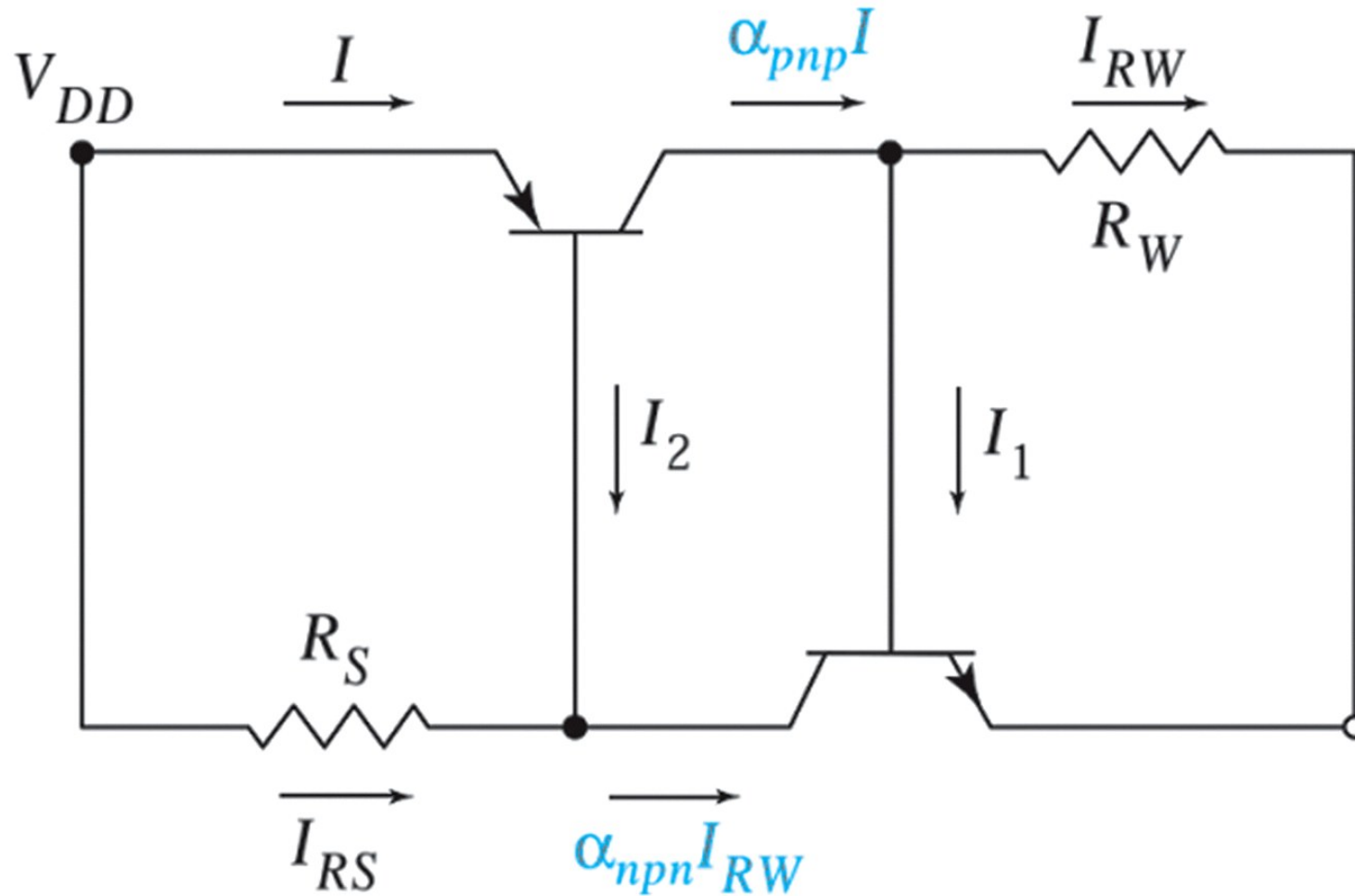


Figure 6.16
 © John Wiley & Sons, Inc. All rights reserved.

Figure 6.16.
 Equivalent circuit of the p -well structure shown in Fig. 15.

如同PNPN結構

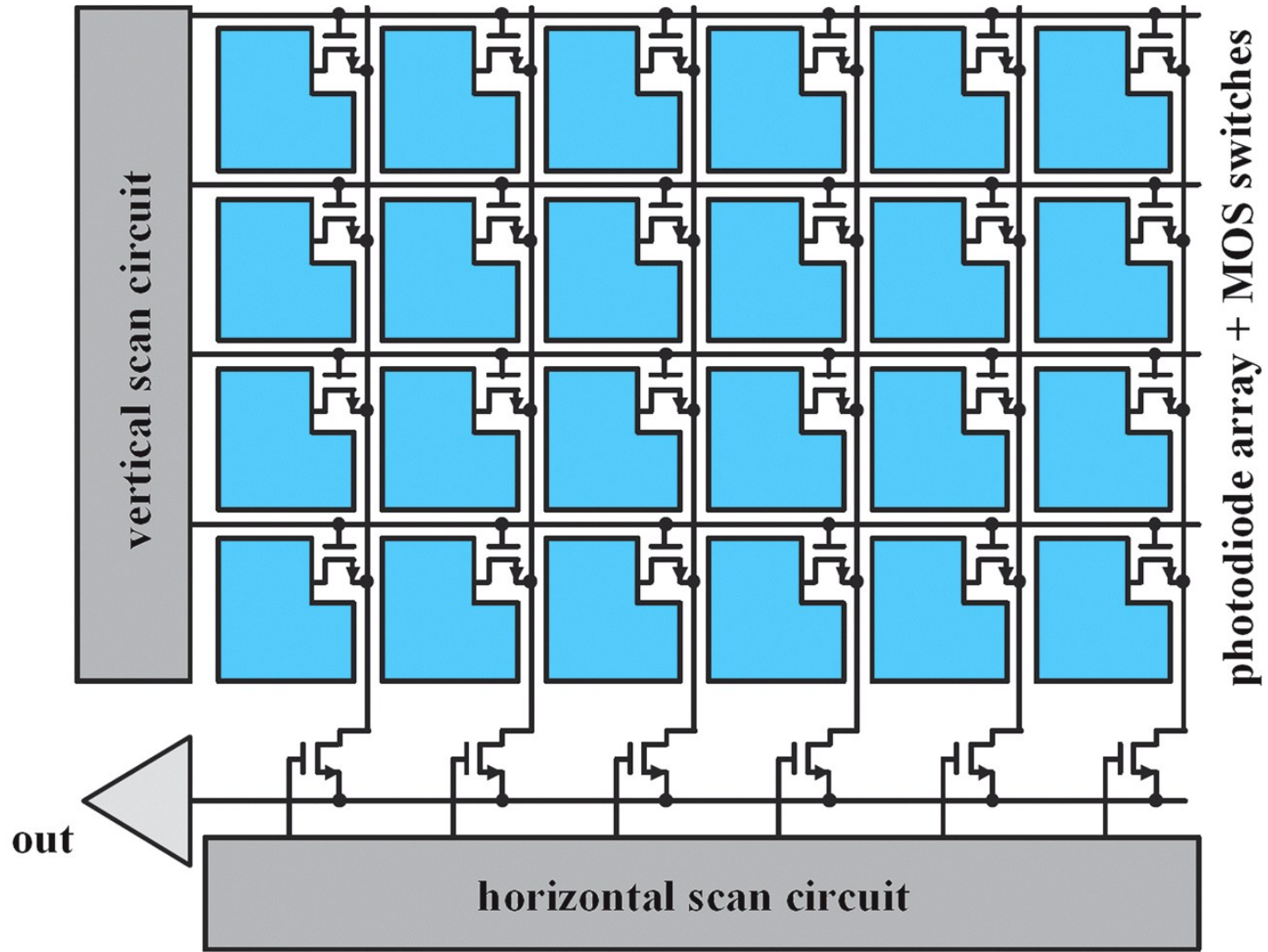


Figure 6.18
 © John Wiley & Sons, Inc. All rights reserved.

2D CMOS image sensor

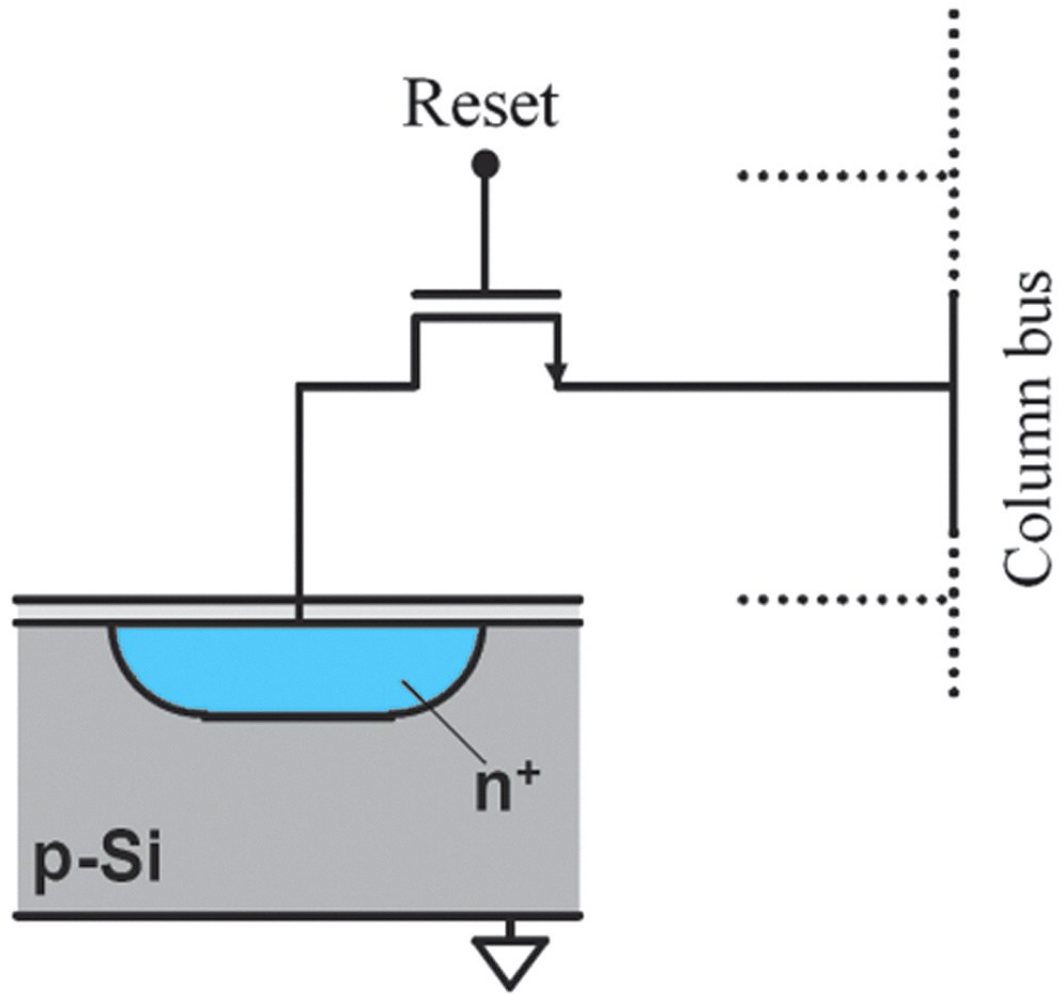


Figure 6.19a
© John Wiley & Sons, Inc. All rights reserved.

Passive CMOS pixel with a single in-pixel transistor

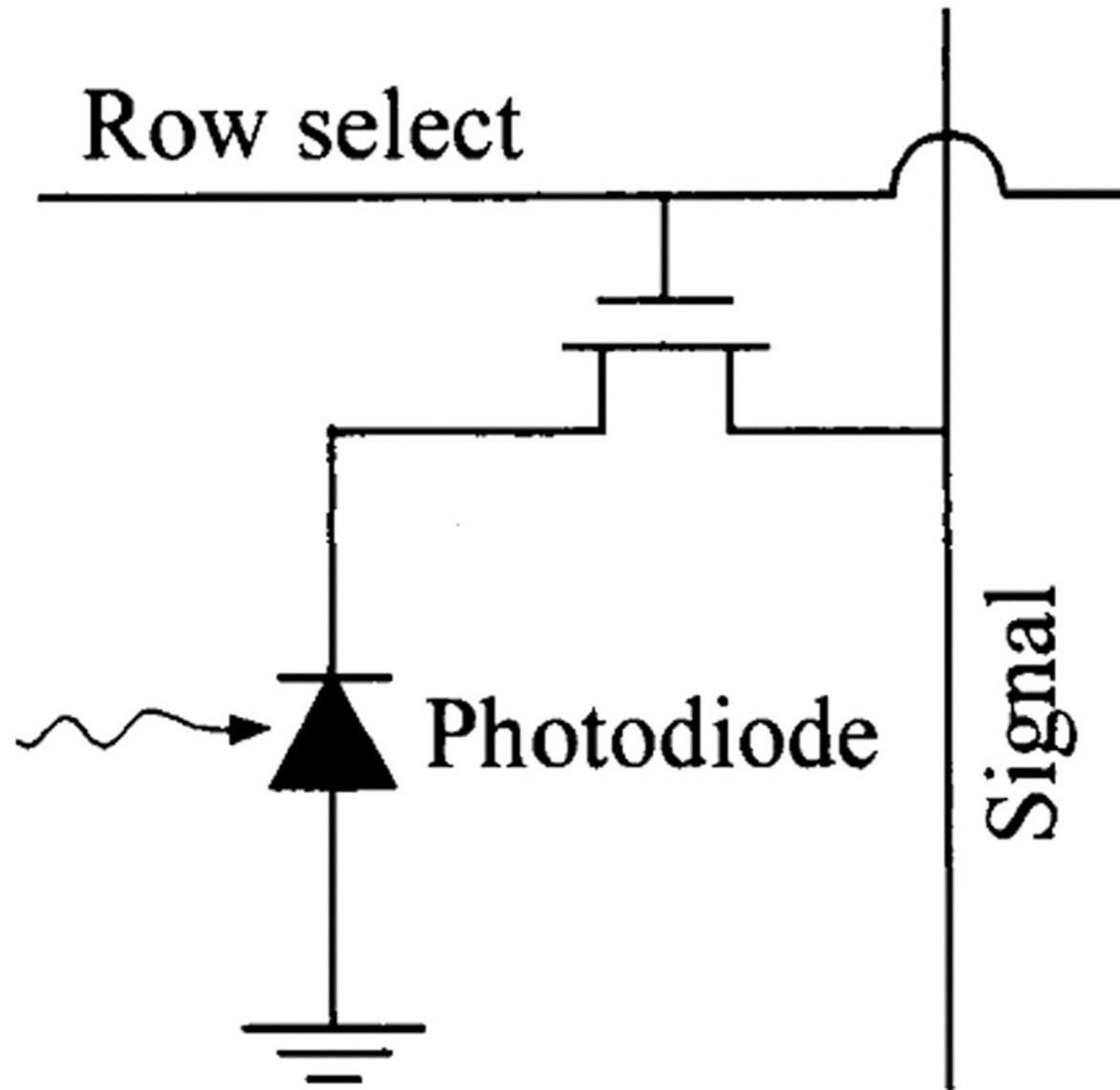


Figure 6.19b
© John Wiley & Sons, Inc. All rights reserved.

Passive pixel sensor CMOS image sensor

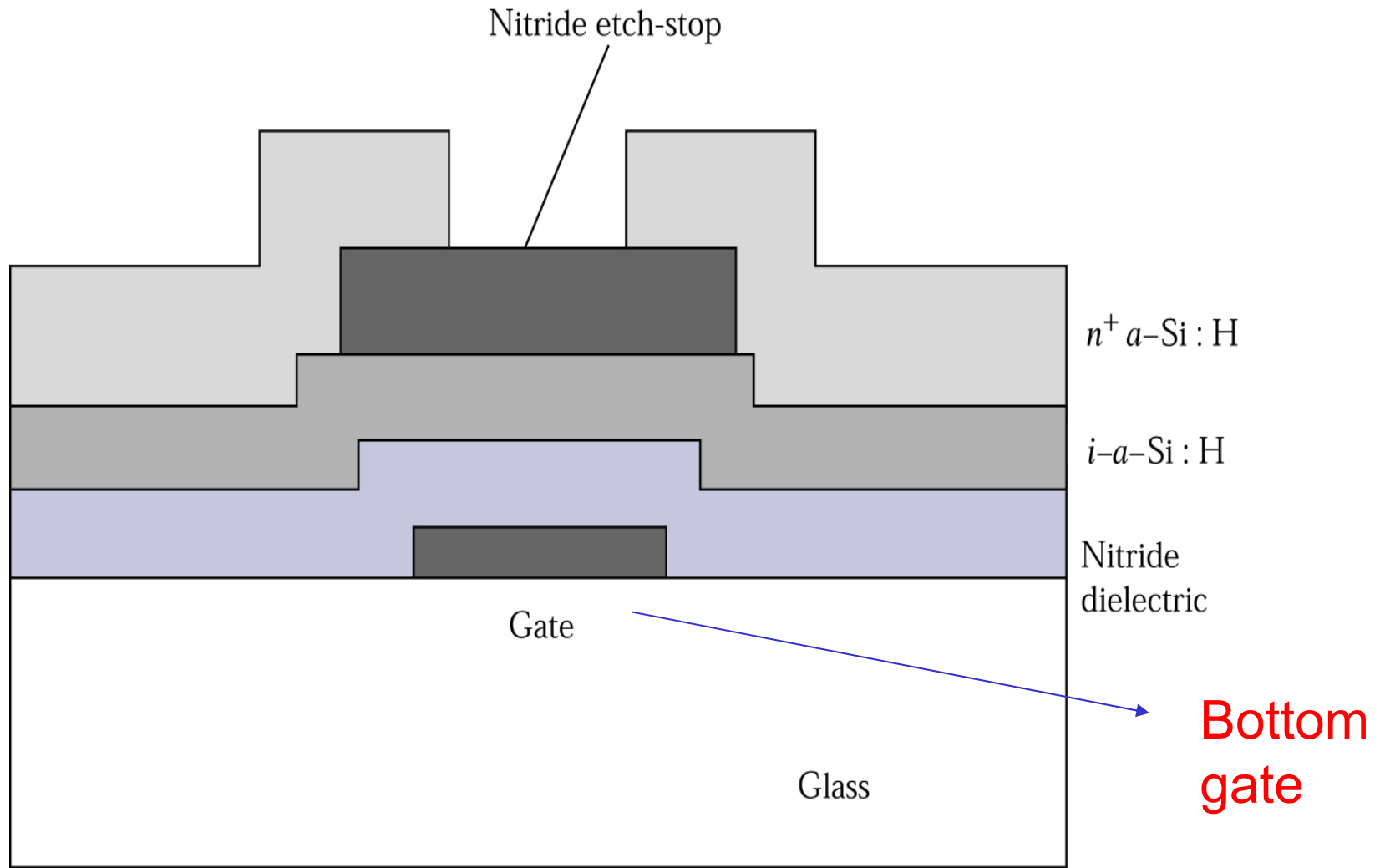
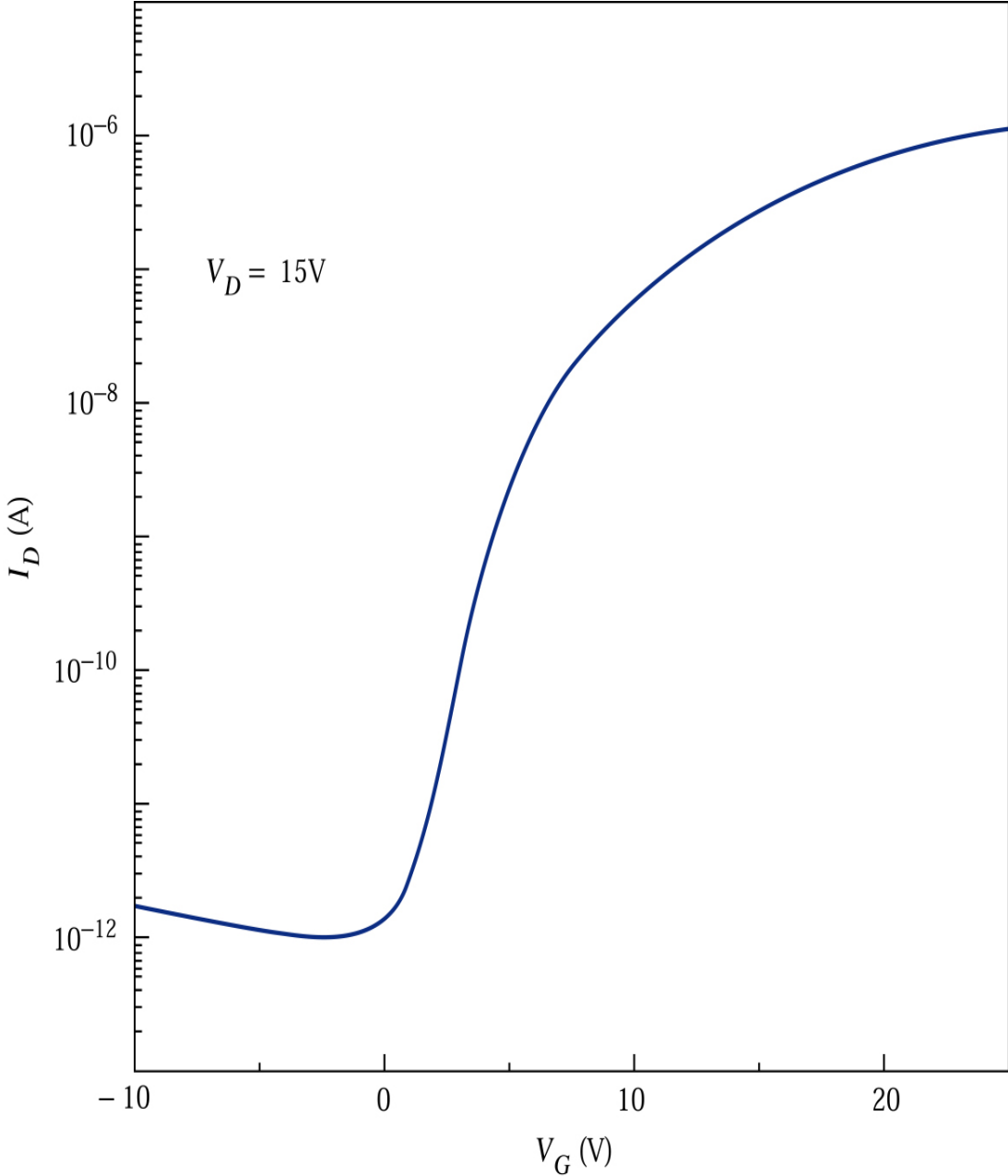


Figure 6.20. A typical **a-Si:H** thin film transistor (TFT) structure.

Figure 6.21.

Subthreshold characteristics of an a-Si:H TFT ($L/Z = 10/60 \mu\text{m}/\mu\text{m}$). The field-effect carrier mobility is $0.23 \text{ cm}^2/\text{V}\cdot\text{s}$.



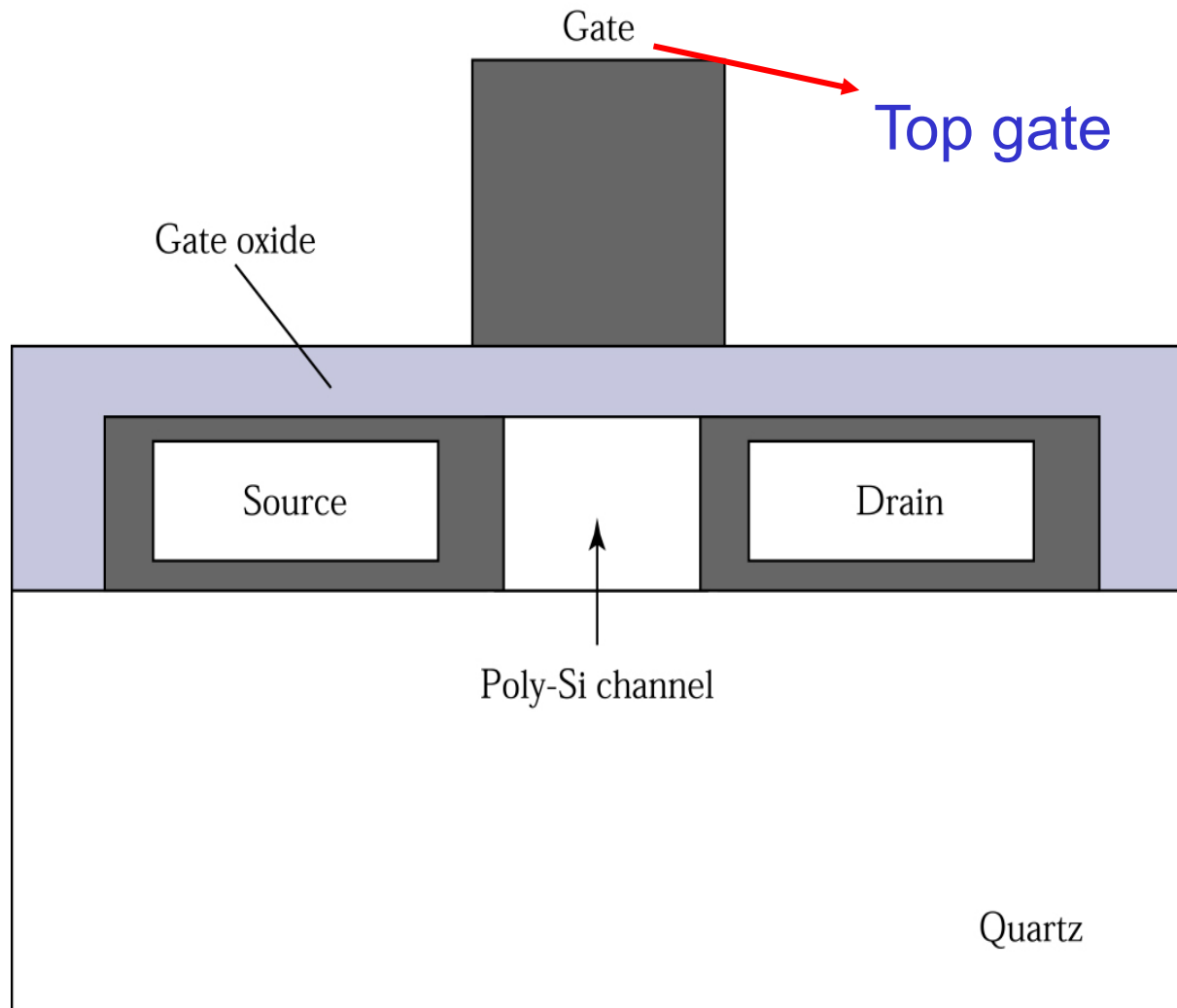
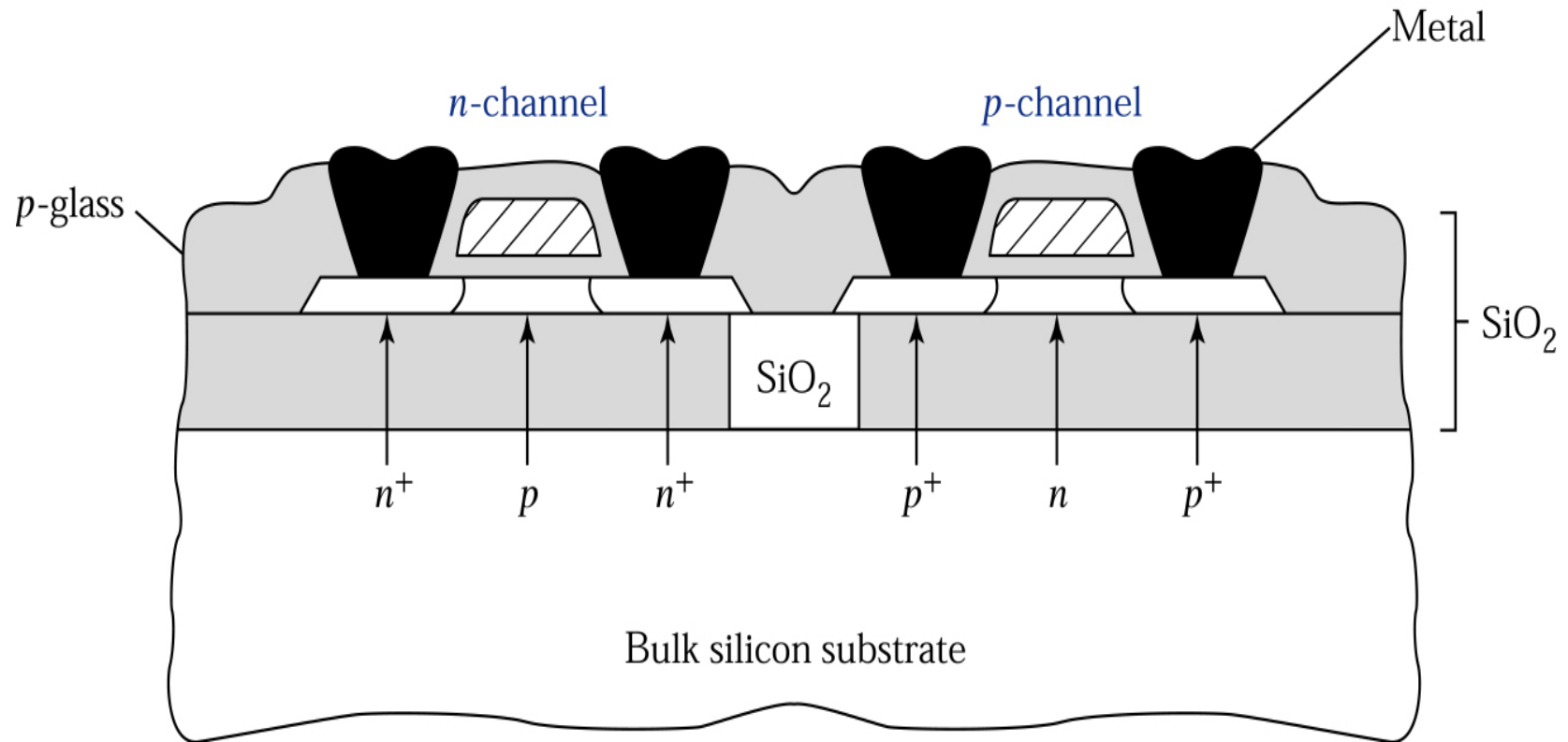


Figure 6.22. A **polysilicon** TFT structure.

Poly-Si, >600C, quartz, expensive, laser annealing



For high freq. application, but SOI wafer is expensive

Figure 6.23. Cross section of the silicon-on-insulator (SOI).

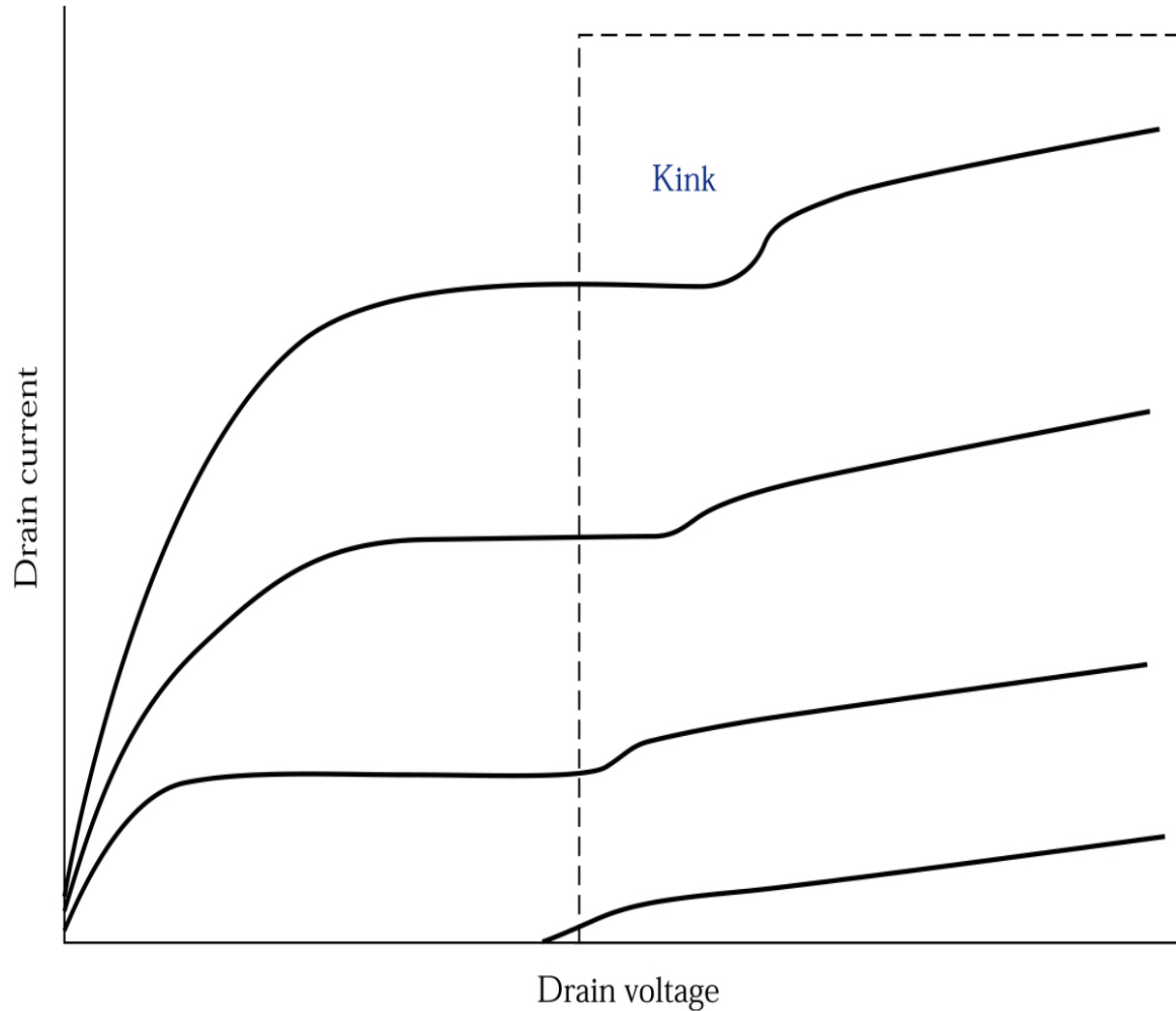
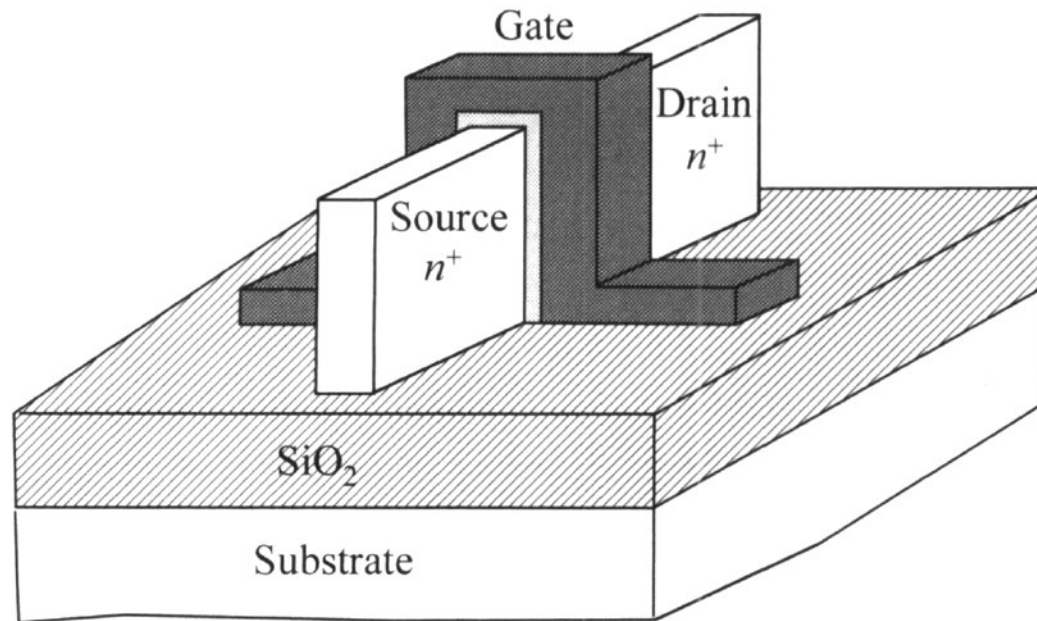
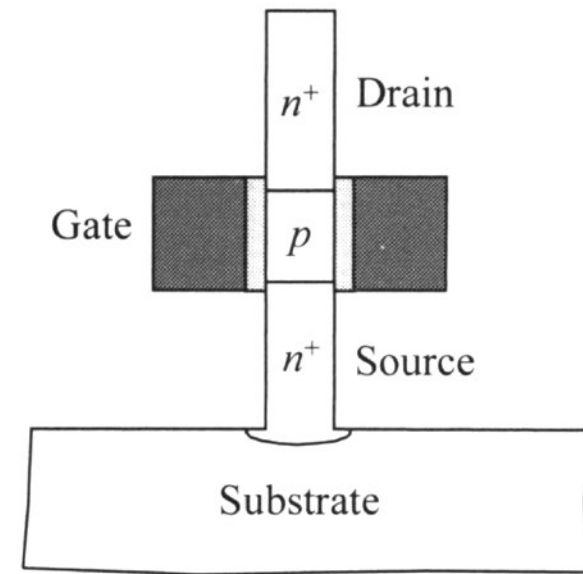


Figure 6.24. The **kink effect** in the output characteristics of an n -channel SOI MOSFET.¹⁵

Hot hole stored in sub, V_b 上升, V_t 減少



(a)



(b)

Figure 6.25
© John Wiley & Sons, Inc. All rights reserved.

3D MOSFET, (a) horizontal (b) vertical structures

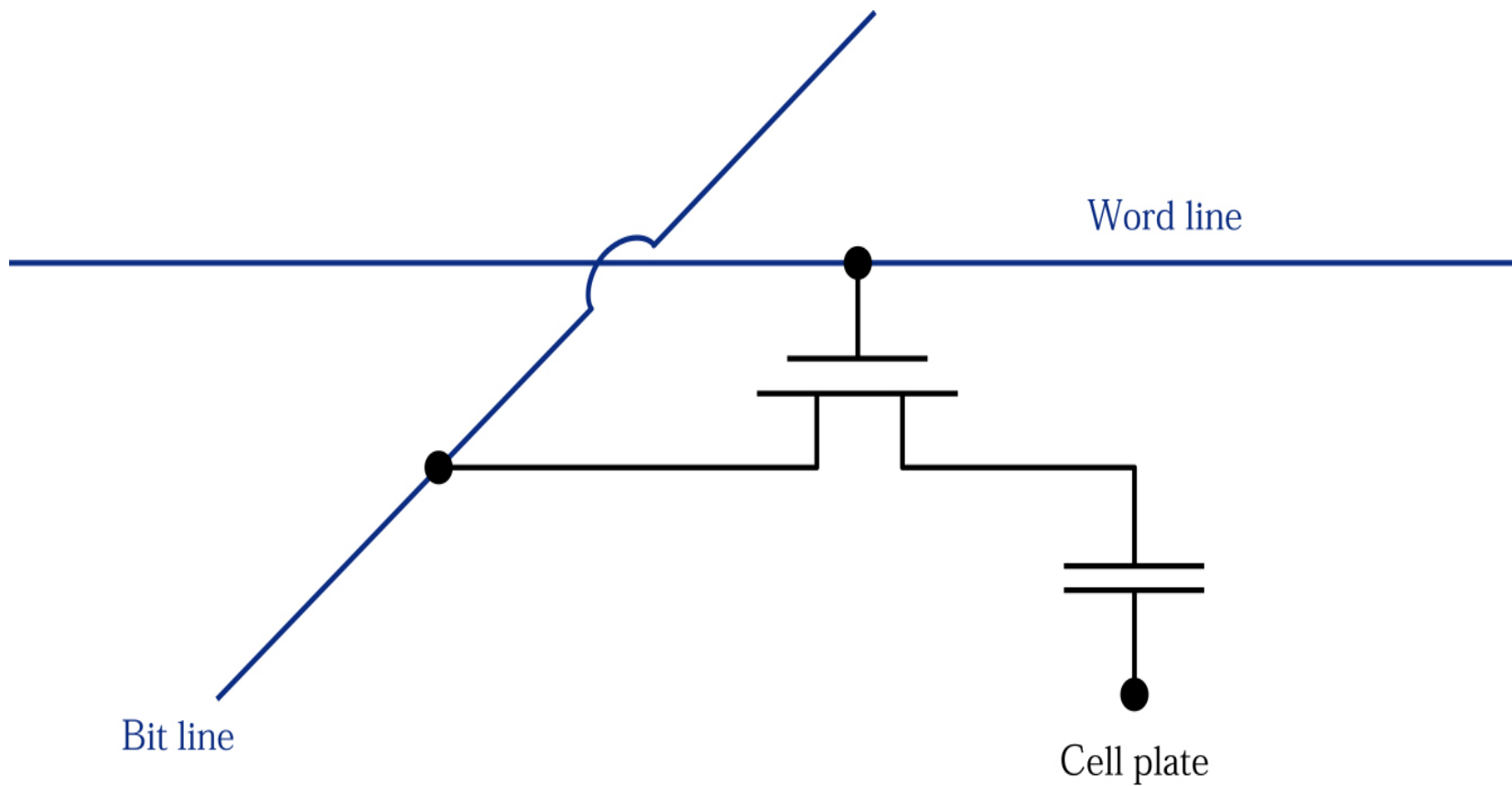


Figure 6.26. Basic configuration of a dynamic random access memory (DRAM) cell.¹⁶

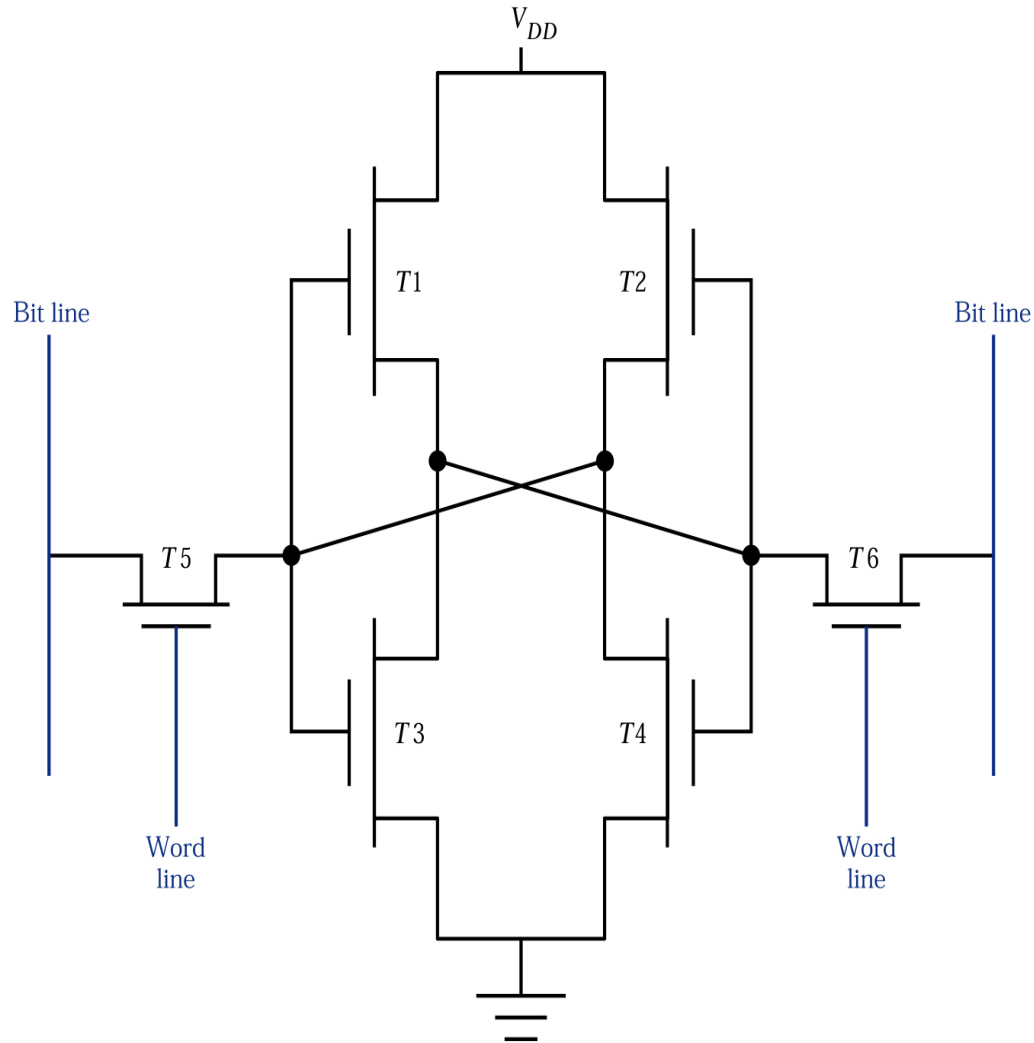


Figure 6.27. Configuration of a CMOS SRAM cell. $T1$ and $T2$ are load transistors (p -channel). $T3$ and $T4$ are drive transistors (n -channel). $T5$ and $T6$ are access transistors (n -channel).

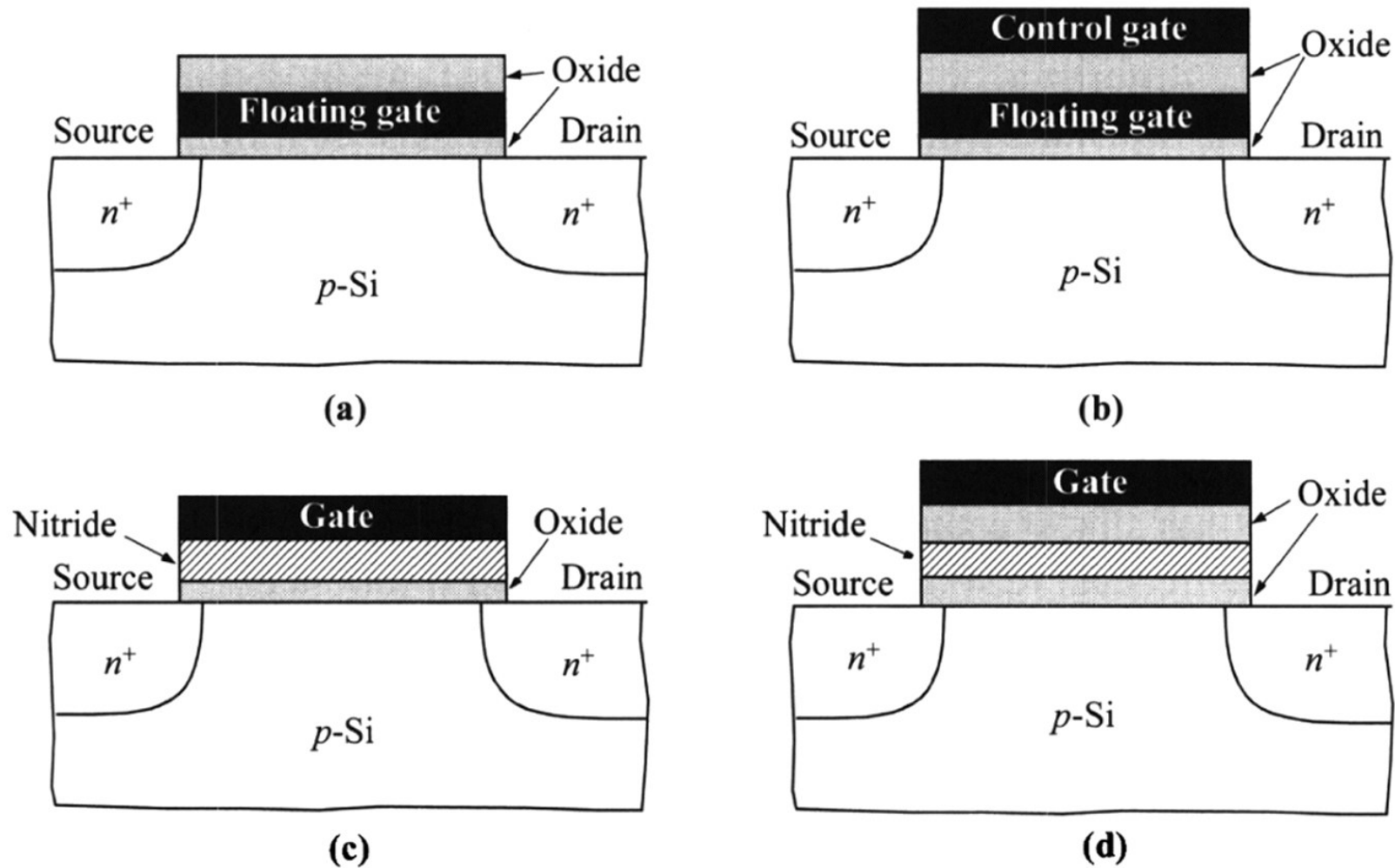


Figure 6.28
 © John Wiley & Sons, Inc. All rights reserved.

Floating gate: (a) FAMOS (b) stacked gate

Charge-trapping : (c) MNOS (d) SONOS

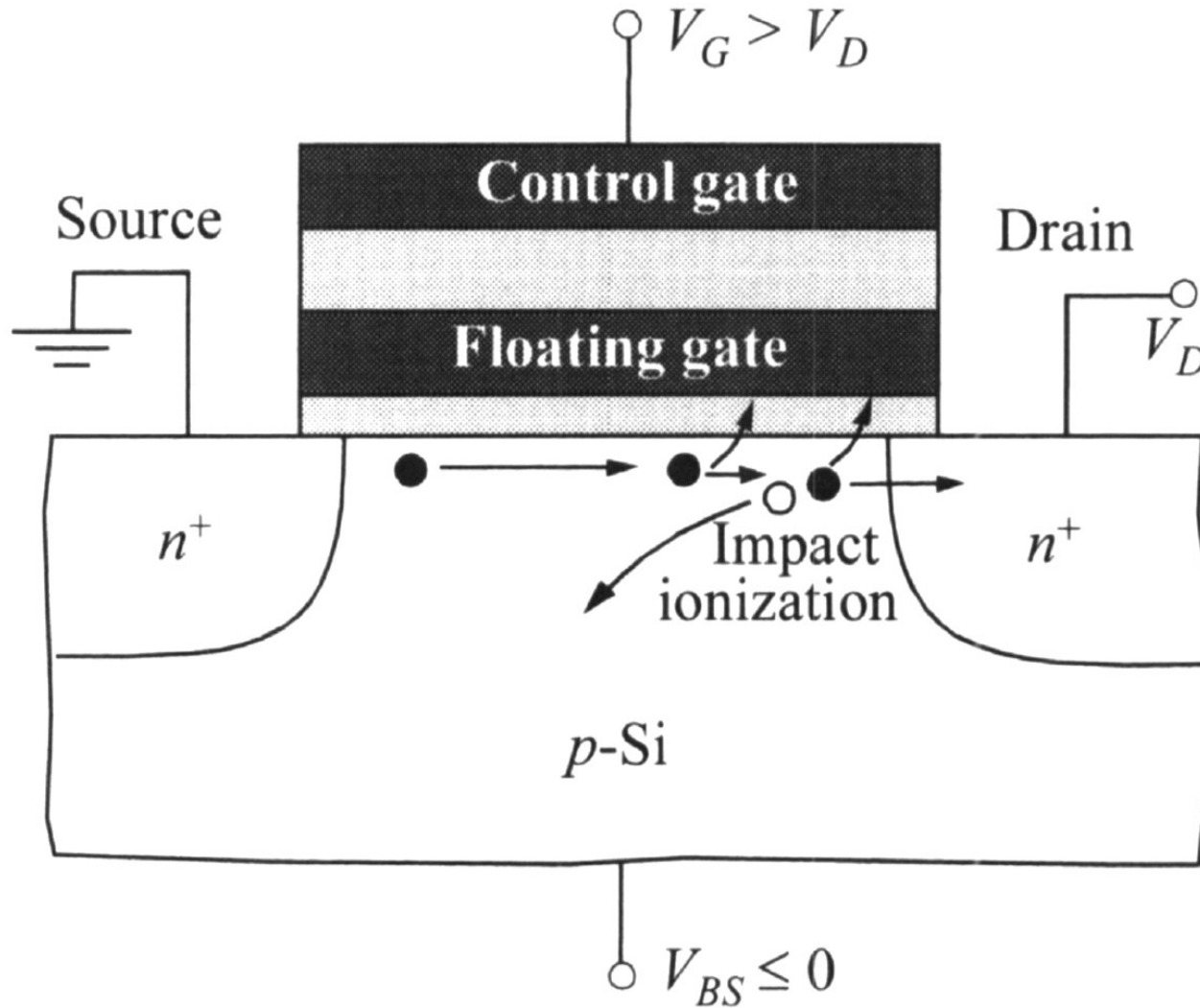


Figure 6.29a
 © John Wiley & Sons, Inc. All rights reserved.

Illustration of hot electron injection in an n-channel, floating-gate nonvolatile memory.

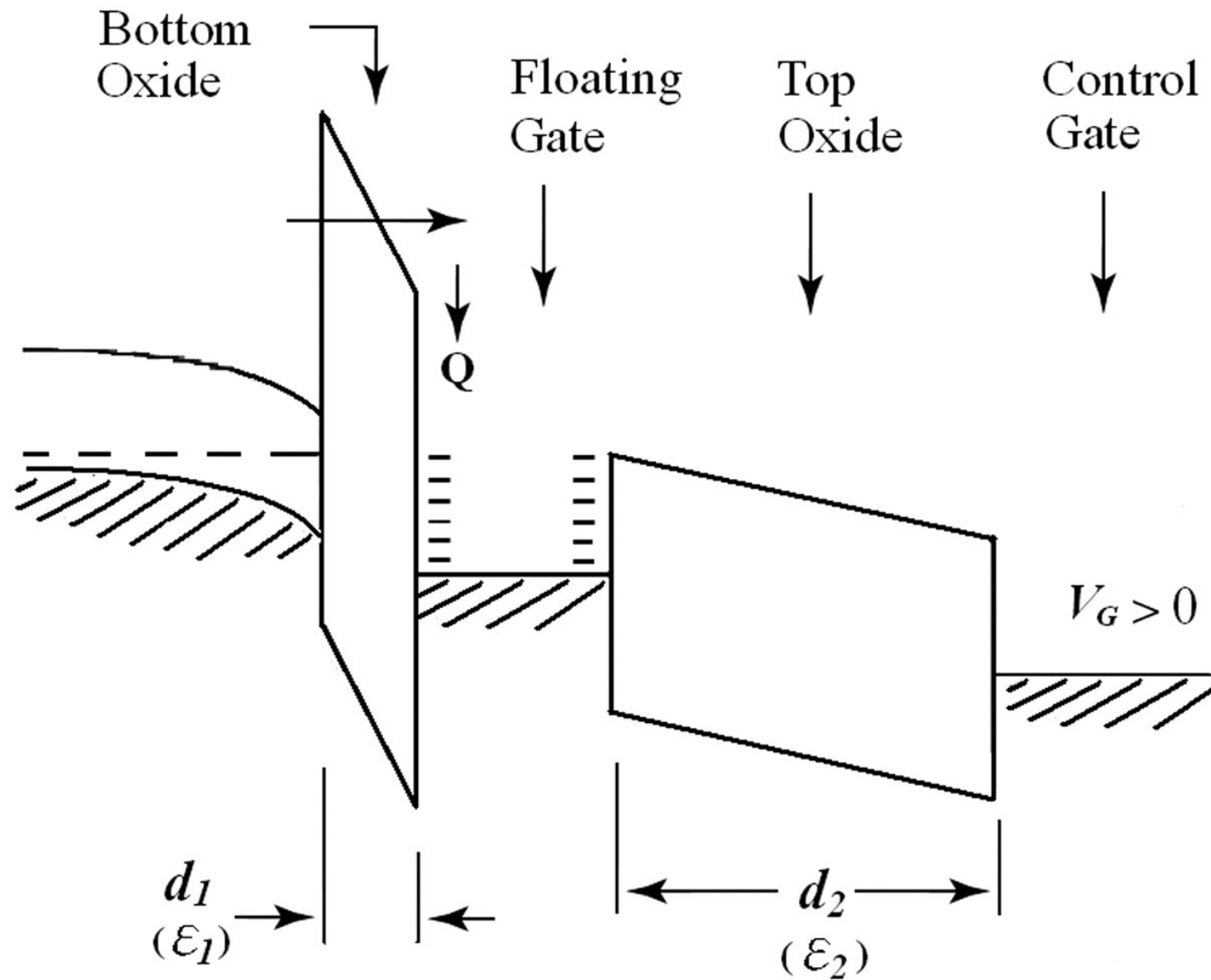


Figure 6.29b
 © John Wiley & Sons, Inc. All rights reserved.

Band diagram of programming condition

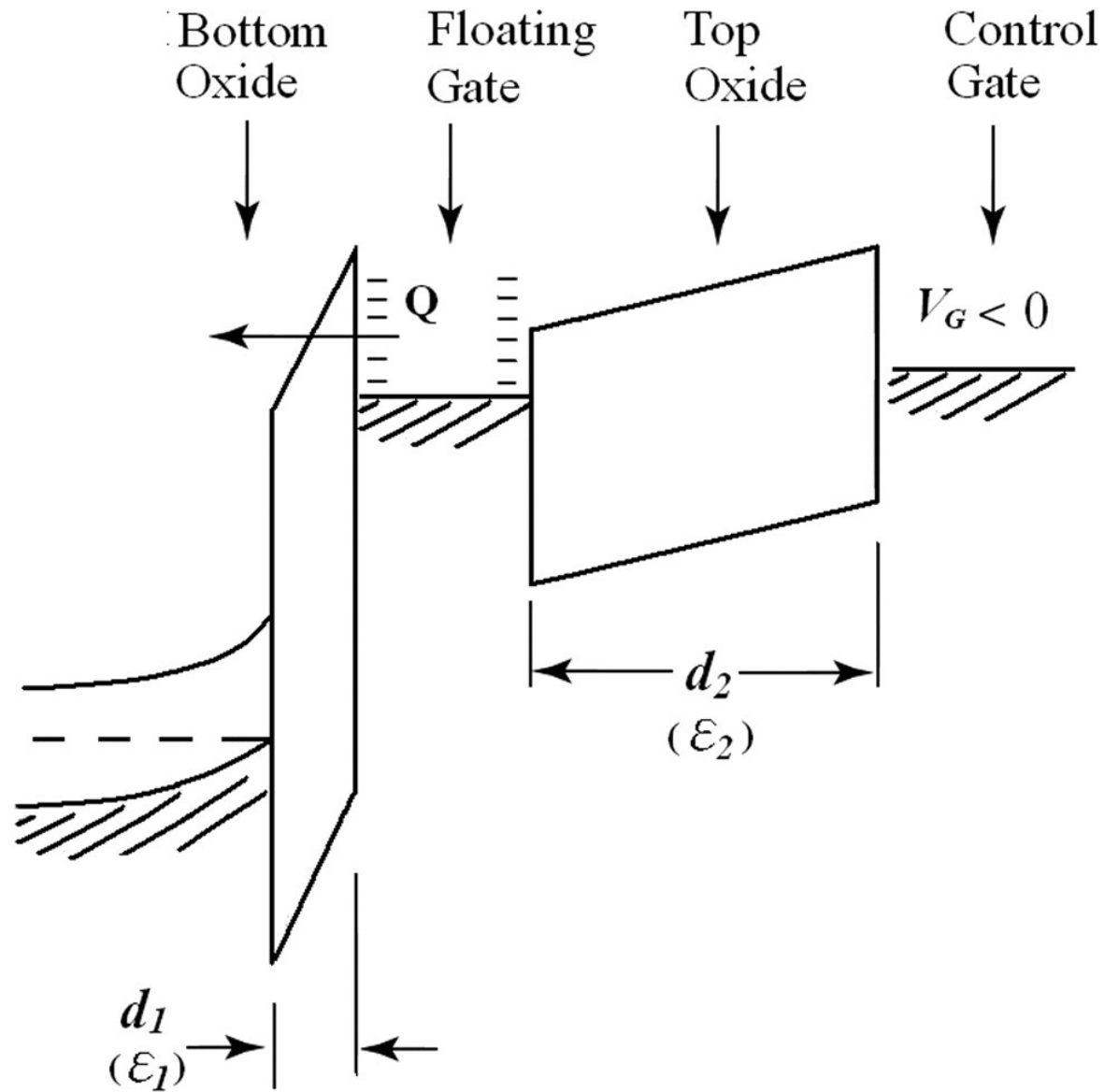


Figure 6.29c
 © John Wiley & Sons, Inc. All rights reserved.

Band diagram of erasing condition

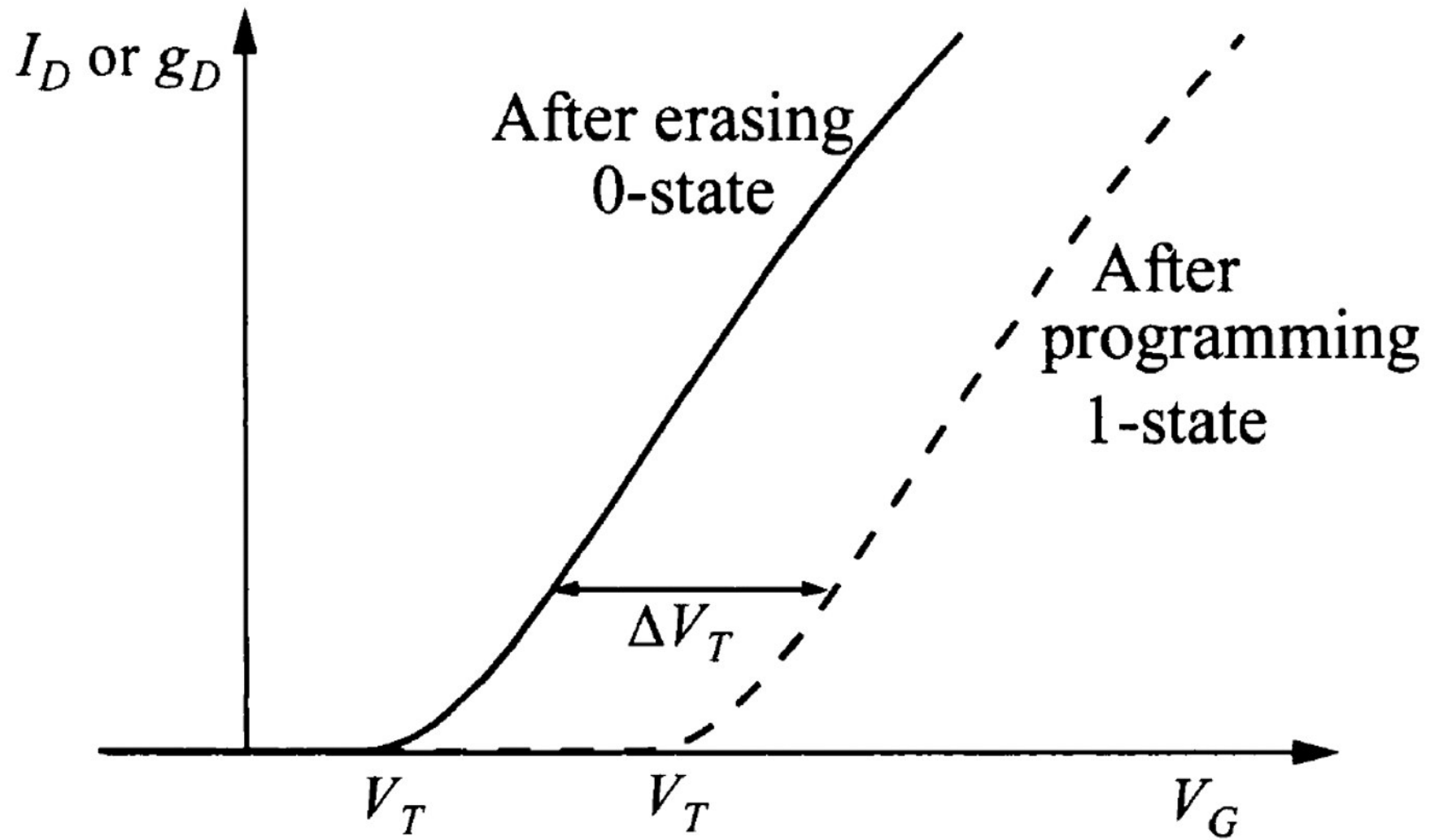


Figure 6.30
© John Wiley & Sons, Inc. All rights reserved.

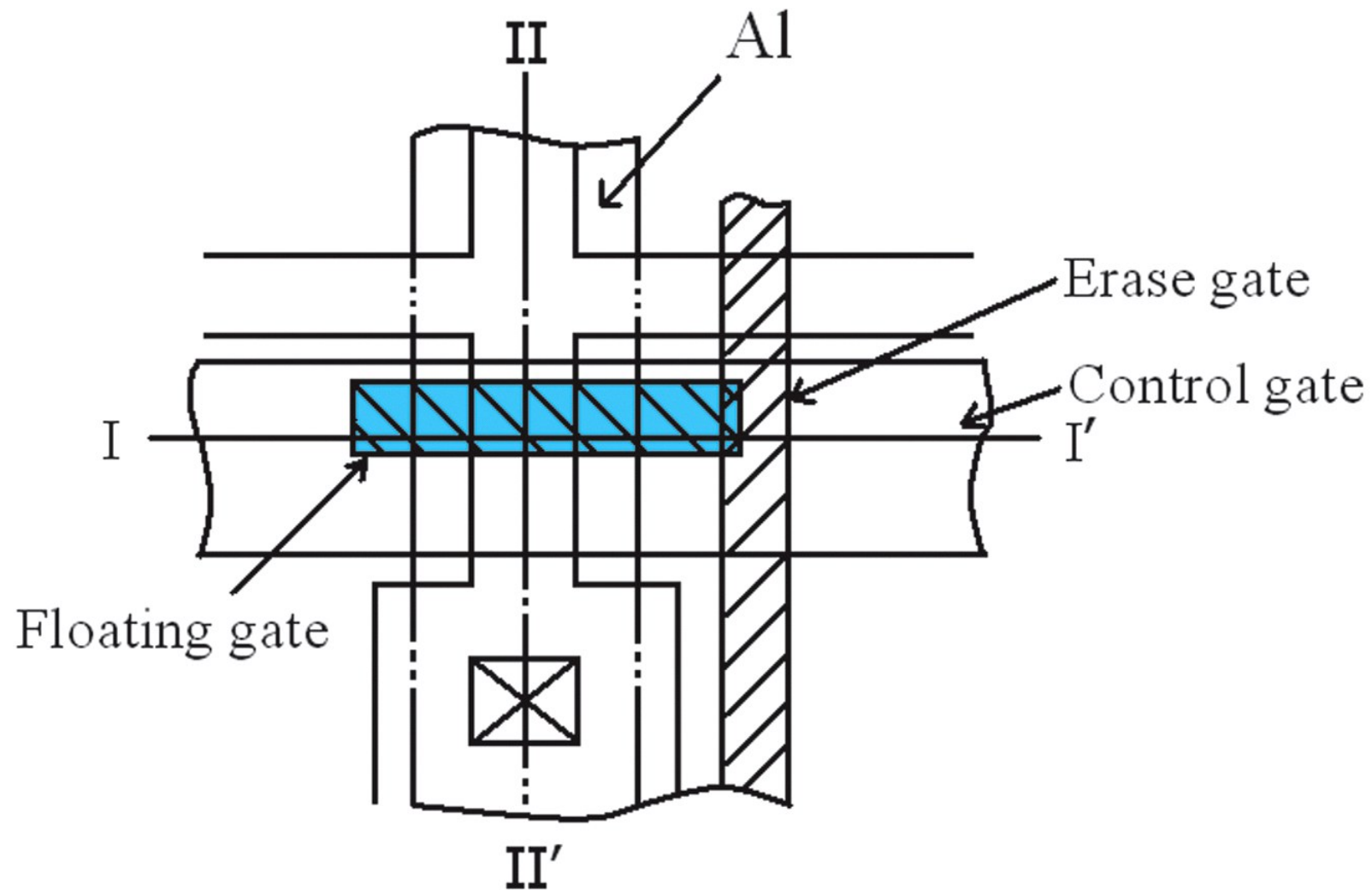


Figure 6.31a

© 1984 IEEE. Reprinted, with permission, from *IEEE Proceedings*, F. Masuoka et. al, "A new flash E2PROM cell using triple polysilicon technology."

Top view of flash memory device

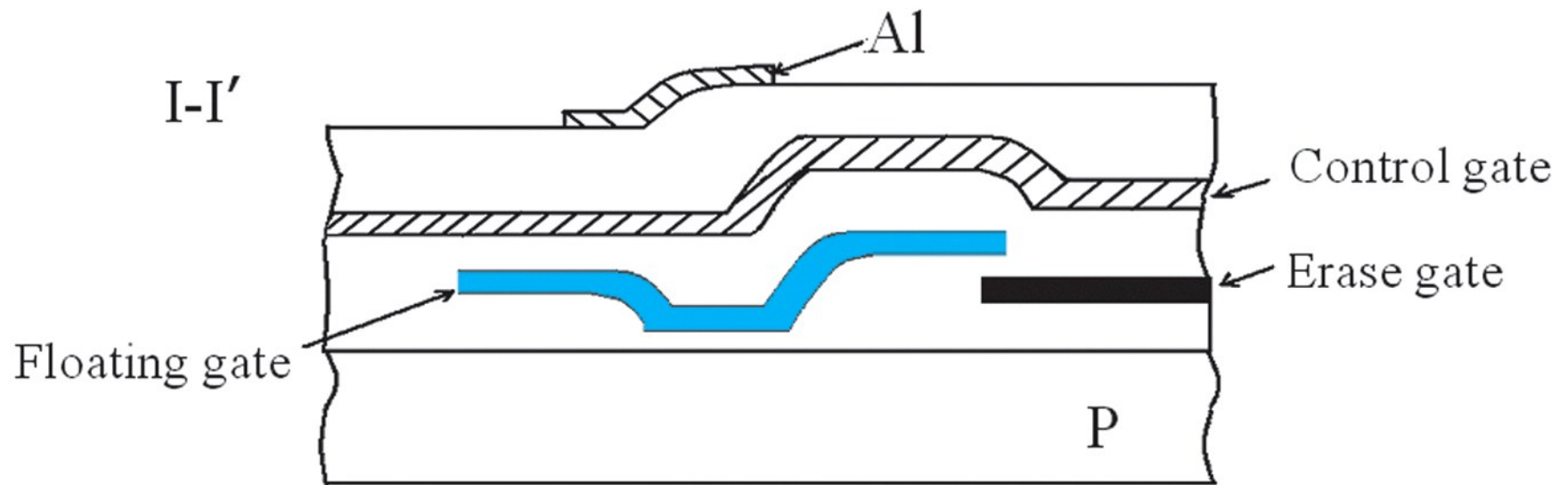


Figure 6.31b
© 1984 IEEE. Reprinted, with permission, from *IEEE Proceedings*, F. Masuoka et. al, "A new flash E2PROM cell using triple polysilicon technology."

Cross-section along I-I' line

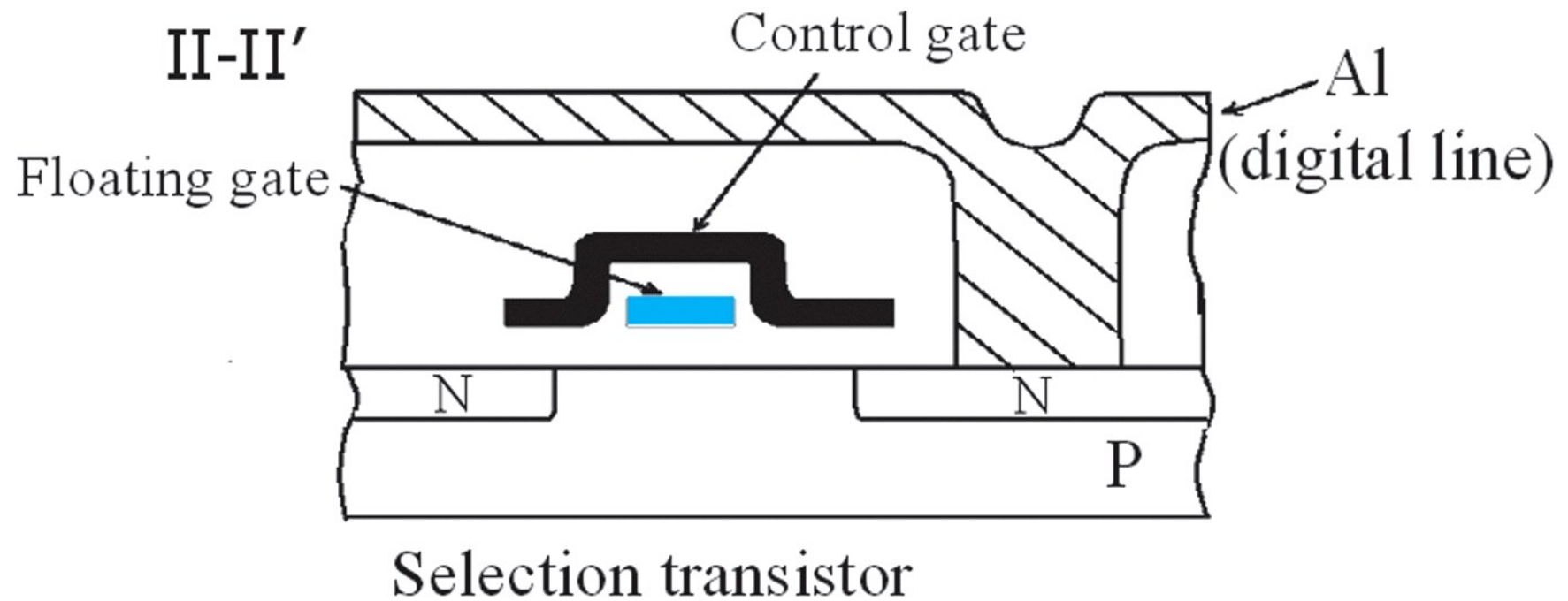


Figure 6.31c

© 1984 IEEE. Reprinted, with permission, from *IEEE Proceedings*, F. Masuoka et. al, "A new flash E2PROM cell using triple polysilicon technology."

Cross-section along II-II' line

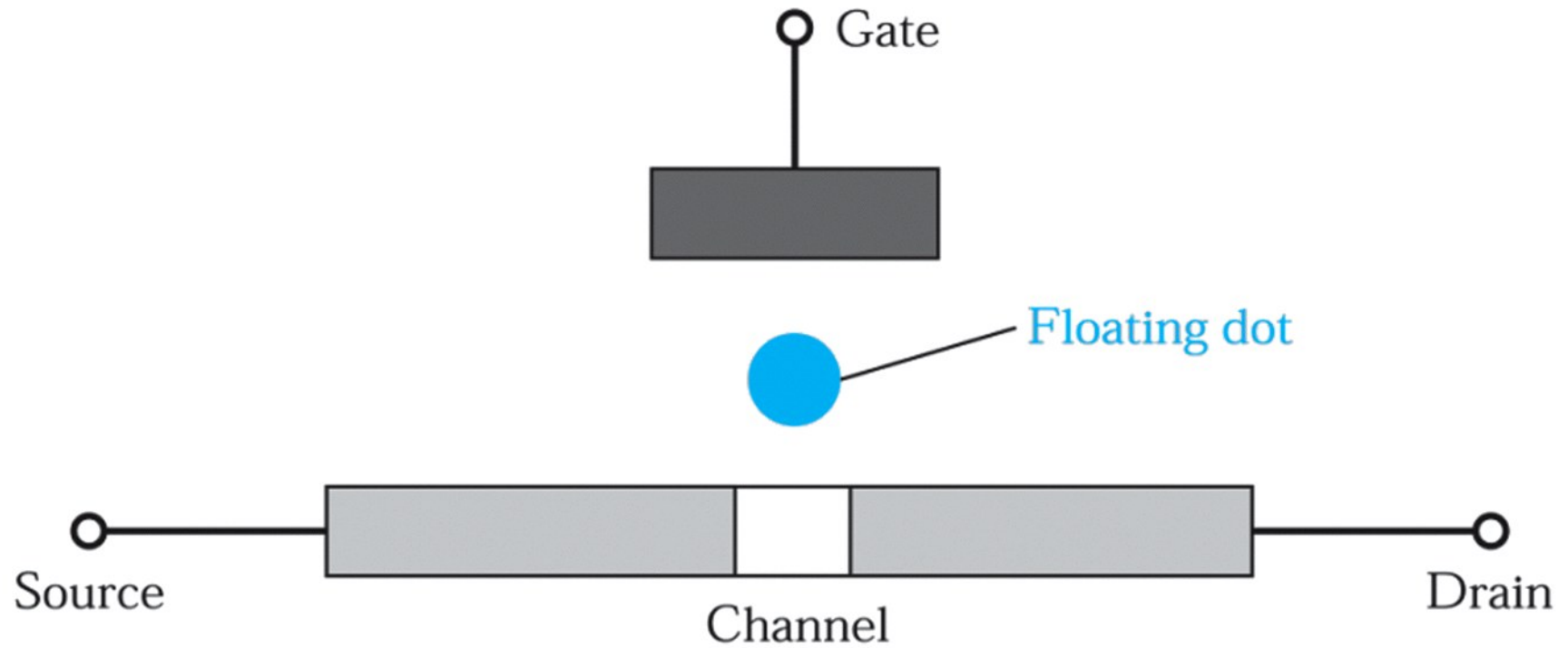


Figure 6.32
© John Wiley & Sons, Inc. All rights reserved.

Single-electron memory cell.

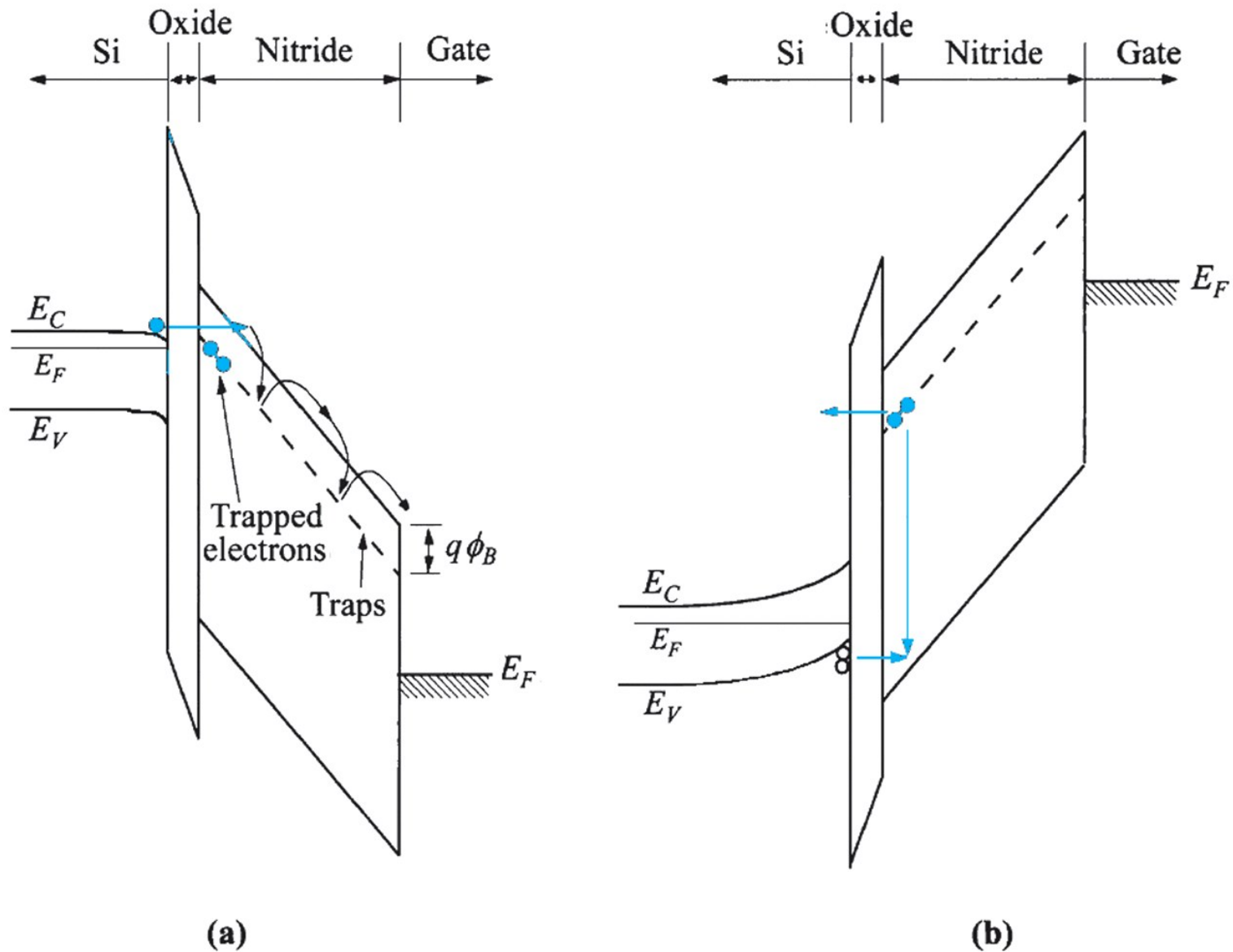


Figure 6.33
 © John Wiley & Sons, Inc. All rights reserved.

MNOS, (a)programming (b)erasing

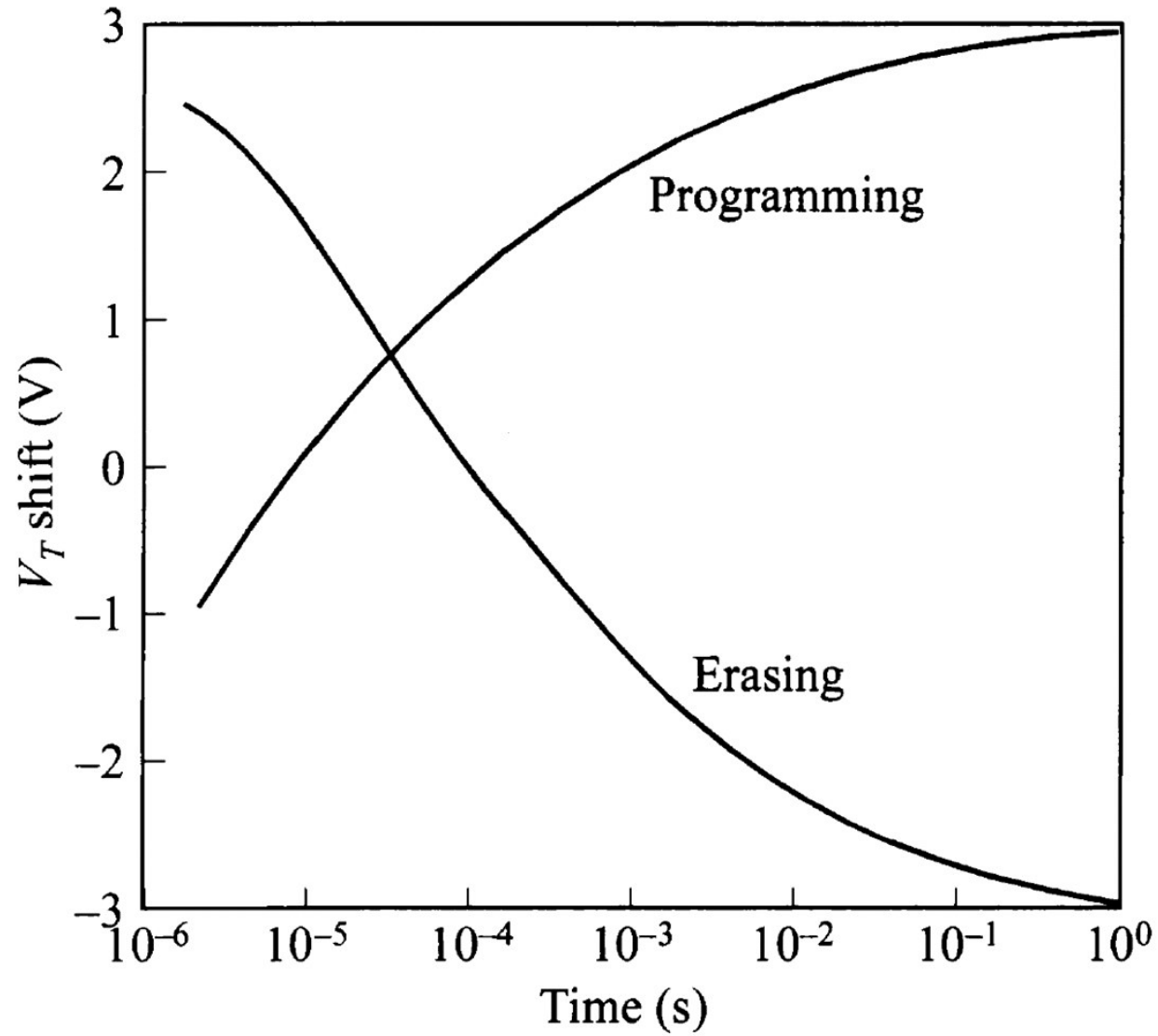
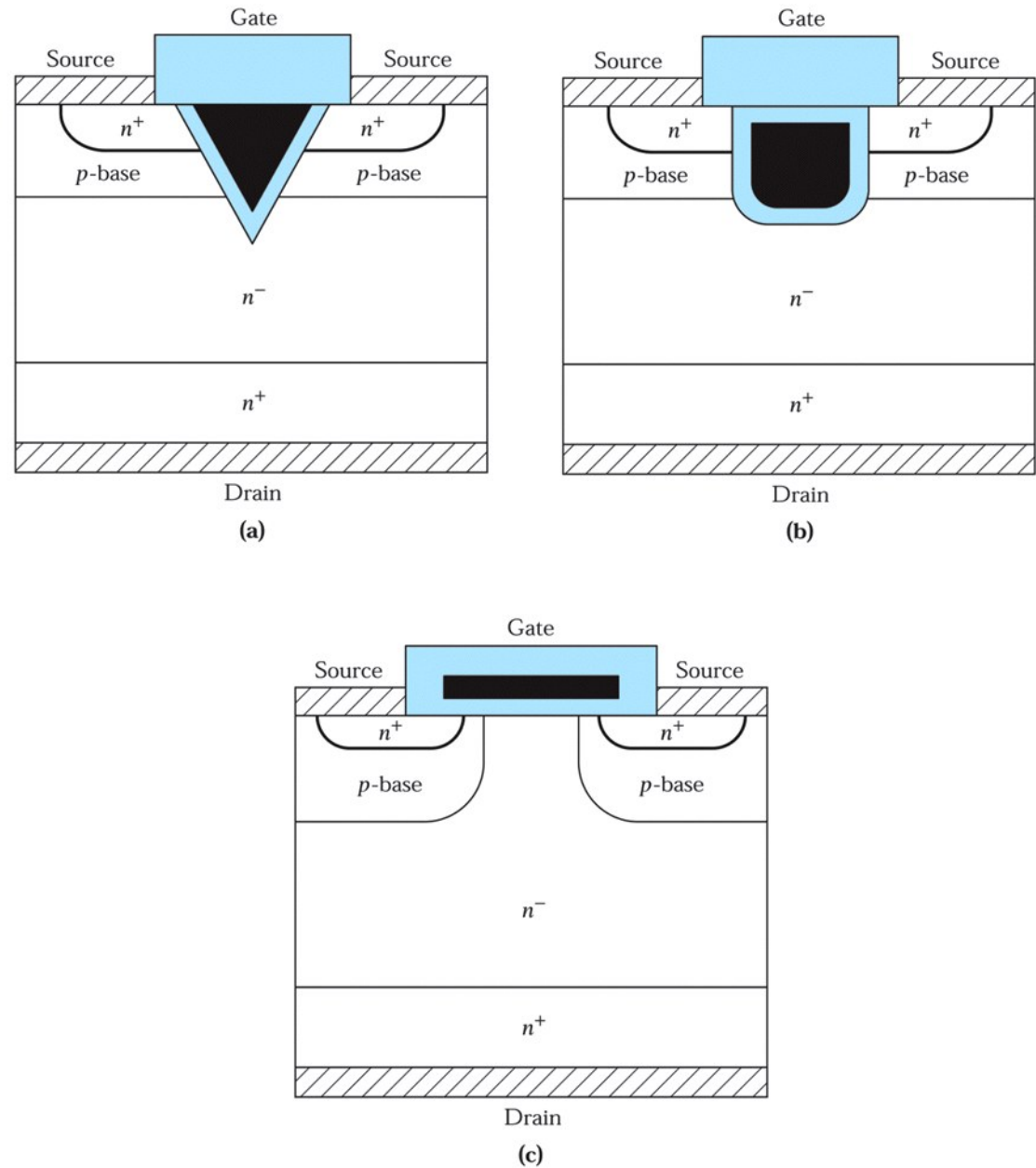


Figure 6.34
© John Wiley & Sons, Inc. All rights reserved.

Programming and erasing rates for MNOS

Figure 6.35.
 (a) V-shaped MOS (VMOS), (b) U-shaped MOS (UMOS), and
 (c) double-diffused MOS (DMOS) power device structures.¹⁹



V_d很大時, n⁻
 depletion, 耐高壓

Figure 6.35
 © John Wiley & Sons, Inc. All rights reserved.

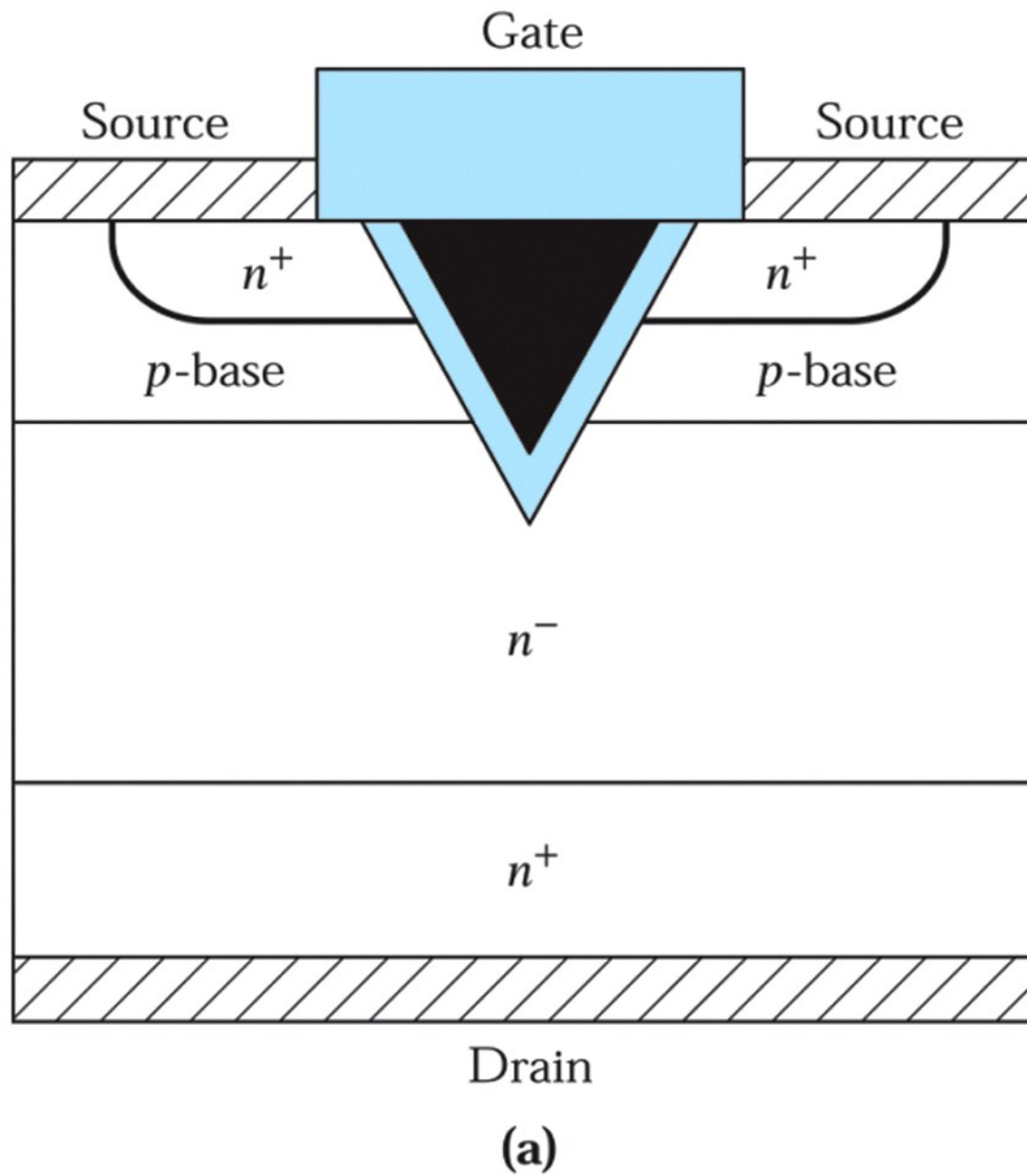


Figure 6.35a
© John Wiley & Sons, Inc. All rights reserved.

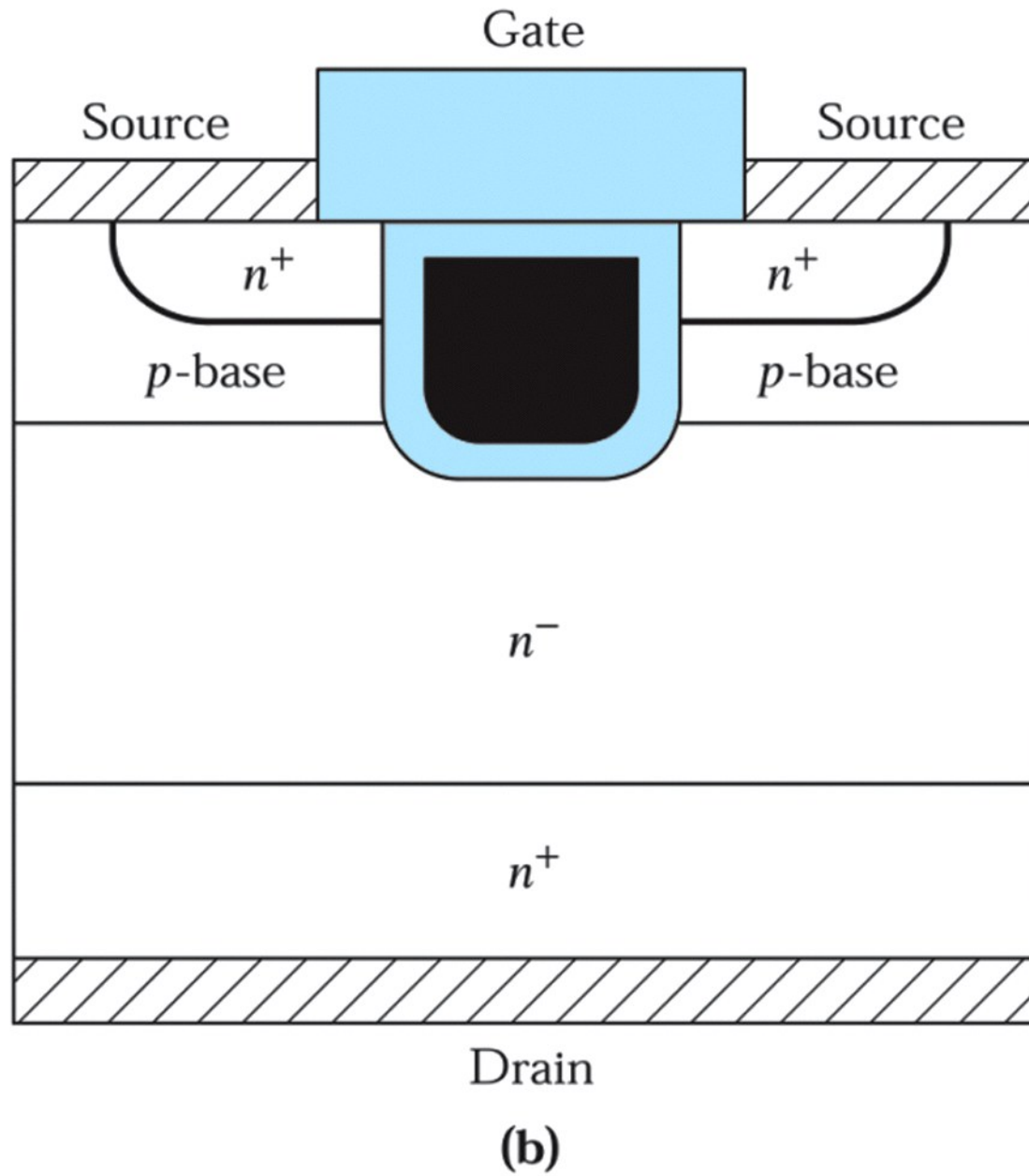


Figure 6.35b
© John Wiley & Sons, Inc. All rights reserved.

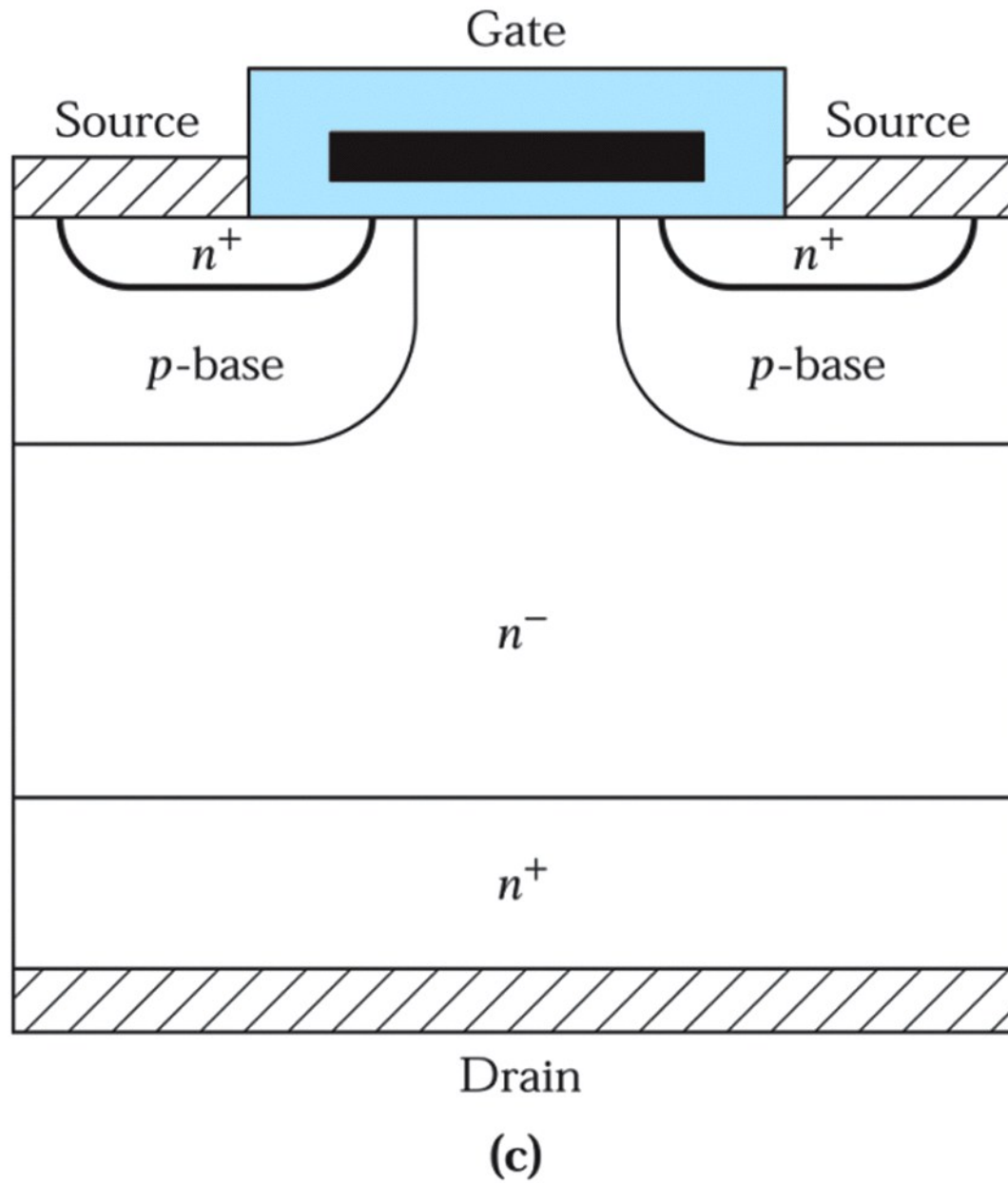


Figure 6.35c
© John Wiley & Sons, Inc. All rights reserved.